INL/RPT-24-77932
Revision 0

Reference Piping and Instrumentation Diagrams for Heat Transport Systems for Methanol Plants

May | 2024

Byung-Hee Choi, Nipun Popli, Sarah Creasman, Ramon Yoshiura, JunSoo Yoo, and Daniel Mikkelson
Idaho National Laboratory

IES
Integrated Energy Systems

INL/RPT-24-77932
Revision 0

Reference Piping and Instrumentation Diagrams for Heat Transport Systems for Methanol Plants

Byung-Hee Choi, Nipun Popli, Sarah Creasman, Ramon Yoshiura, JunSoo Yoo, and Daniel Mikkelson
Idaho National Laboratory

May | 2024

Idaho National Laboratory
Integrated Energy Systems
Idaho Falls, Idaho 83415

http://www.ies.inl.gov

Prepared for the
U.S. Department of Energy
Office of Nuclear Energy
Under DOE Idaho Operations Office
Contract DE-AC07-05ID14517

Page intentionally left blank

EXECUTIVE SUMMARY

Key Research Question

Interest in industrial decarbonization is driving innovation in integrated energy systems (IESs) centered on advanced nuclear reactors. These IESs aim to deliver clean energy from nuclear reactors to meet the industrial sector's thermal and electrical demands using novel process pathways for decarbonization. This report investigates the integration of advanced nuclear reactors with non-traditional methanol production facilities.

Research Overview

Methanol producers seeking decarbonization using advanced nuclear power can use the tools and information provided in this report to guide efforts to integrate clean nuclear heat into novel methanol production processes. This work follows a three-step approach:

1. Modeling of Traditional and Decarbonized Processes for Methanol Production.
    - Process models of two novel methanol production pathways, with their overall energy requirements, are compared to traditional methanol production designs (see Figure ES-1.). These process models provide the foundation for analyzing combined heat and power (CHP) systems for coupling advanced methanol plants with advanced nuclear reactors.
2. Identification of Coupling Points to Integrate Advanced Reactors.
    - The coupling points between advanced methanol plants and advanced nuclear plants are identified. This report investigates integration of two advanced reactor technologies: light-water reactors (LWRs) and high-temperature gas reactors (HTGRs) to advanced methanol plants.
3. Thermal Coupling Design Development for Preliminary Heat and Electricity Transfer from Reactors to Methanol Production Sites.
    - Piping and instrumentation diagrams (P&IDs) are developed for reference designs to transfer heat from advanced reactors to the coupling point, such as a steam header, at the methanol plant site. The pipe analysis for thermal coupling design complies with relevant codes and specifications from American Society of Mechanical Engineering (ASME).

Key Findings

A key step to methanol synthesis is production of syngas, which is a mixture of carbon monoxide and hydrogen. Use of nuclear energy in syngas preparation provides an opportunity to completely replace natural gas as a feedstock through the introduction of a reverse water gas shift (RWGS) reactor. Figure ES-1. shows the net energy requirements for traditional methanol production, clean heating of steam-methane reformer via hydrogen burning instead of using natural gas, and complete elimination of natural gas usage as feedstock via RWGS. Corresponding net emissions including scope-1 site emissions and an assumed burning of final synthesized methanol are shown in Figure ES-2., which shows a 17.3% reduction in emissions through steam-methane reforming heat replacement and a circular carbon methanol economy from the RWGS.

Both LWRs and HTGRs are identified as capable of meeting the energy needs for both processes, as viable configurations either consume purchased natural gas or light-gas byproducts of the methanol plant for internal heat demands. The nuclear systems interface entirely via hydrogen production, which for optimal efficiency is high-temperature steam electrolysis.

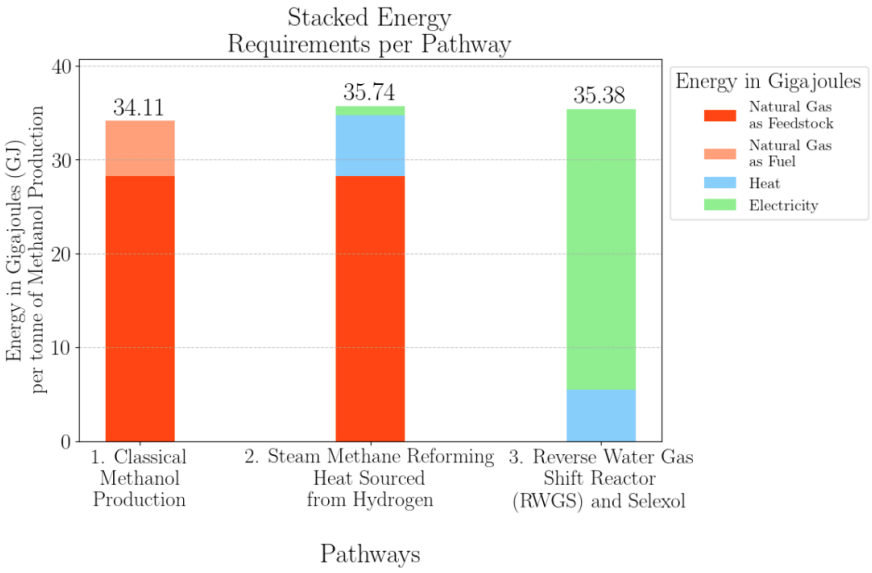

Figure ES-1. Comparative chart of energy required per tonne production of methanol under three scenarios: (a) Nominal: Production at mega-methanol plants with steam-methane reforming and auto-thermal reforming, using natural gas as a feedstock for synthetic gas production and as a fuel to power burners or furnaces, (b) Pathway-1: Replacement of natural gas with hydrogen as a fuel for the purpose of powering burners or furnaces, and, (c) Pathway-2: Replacement of natural gas with hydrogen as a fuel in burners or furnaces, and as a feedstock for synthetic gas production.

This Matters

Methanol is a common feedstock for many chemicals including potentially synthetic fuels such as gasoline or jet fuel. An opportunity to dramatically reduce the emissions of methanol synthesis—through an assumed use that produces carbon such as liquid fuel consumption—provides a significant global decarbonization opportunity as well as a potential pathway toward commercialization for novel nuclear designs. Electrolysis via electricity from nuclear power plants has been thoroughly pursued and demonstrations are beginning to split water; additional facilities are also planned for the near future.

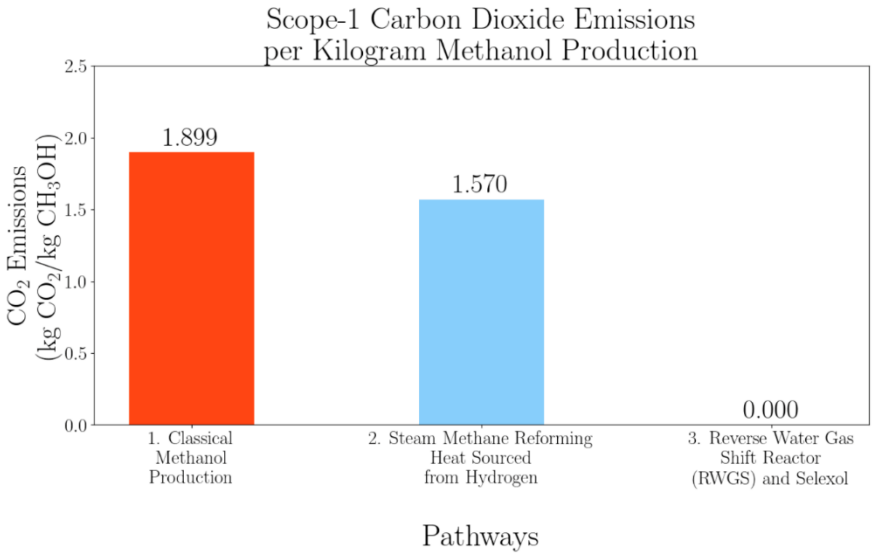

Figure ES-2. Total scope 1 and eventual assumed methanol end use that produces CO_2.

How to Apply Results

Multiple applications are foreseen for these results. The cleaner methanol pathways present preliminary concepts for advanced methanol facilities that can maintain operation in a decarbonized economy. The requirements for both the internal facility mass and energy flows as well as the required external energy inputs can be leveraged for future configurations. Most importantly, these designs provide sufficient information with regard to pressures, contents, and flows so that economic evaluations of the proposed pathways can be made.

Page intentionally left blank

CONTENTS

FIGURES

TABLES

Page intentionally left blank

LIST OF ACRONYMS

AF	Amortization factor
ASME	American Society of Mechanical Engineers
ATR	Auto-thermal reforming
BOP	balance of plant
CFM	cubic feet per minute
CHP	combined heat and power
DEPG	Dimethyl Ethers of Polyethylene Glycols
GHG	greenhouse gas
HTF	heat transfer fluid
HTGR	high-temperature gas-cooled reactor
HTSE	High-Temperature Steam Electrolysis
IES	integrated energy system
INL	Idaho National Laboratory
LWR	light-water reactor
MeOH	methanol
MMT	million metric tons
NG	Natural gas
NPM	NuScale Power Module
NPP	Nuclear power plant
NPS	Nominal pipe sizes
P&ID	Piping and instrumentation diagram
RWGS	Reverse Water Gas Shift
SMR	steam-methane reforming
SOEC	Solid Oxide Electrolyzer Cell
tpd	tonne per day

Page intentionally left blank

Reference Piping and Instrumentation Diagrams for Heat Transport Systems for Methanol Plants

1. INTRODUCTION

The Integrated Energy Systems (IES) Program within the Department of Energy is targeting decarbonization in industrial processes, with one of the main focus areas being methanol production. Methanol serves not only as a fuel but also as a crucial building block for various chemicals like plastics, paints, olefins, or for production of synthetic fuel such as gasoline and jet fuel [1, 2]. Despite having a lower volumetric energy density than gasoline (roughly half), methanol's liquid form has a potential to facilitate transportation through existing infrastructure. Additionally, it also allows for practical large-scale storage. Hence, methanol offers advantages for both transportation and storage of energy.

The IES program at Idaho National Laboratory (INL) is investigating the use of advanced nuclear reactors to displace fossil fuels in methanol production. Traditionally, natural gas serves as a critical feedstock and fuel for methanol production. The rise of shale gas production in the United States (U.S.) since 2005 has fueled a significant increase in methanol production [3]. As illustrated in Figure 1, U.S. methanol output grew nearly eightfold to 5 million metric tons (MMT) between 2010 and 2019, coinciding with a surge in shale gas and a decrease in natural gas prices. The increased use of natural gas potentially amounts to an average of 9.5 MMT of carbon dioxide emission per annum. Replacing natural gas with clean nuclear energy and exploring alternative pathways for methanol production are critical steps toward decarbonizing methanol production facilities.

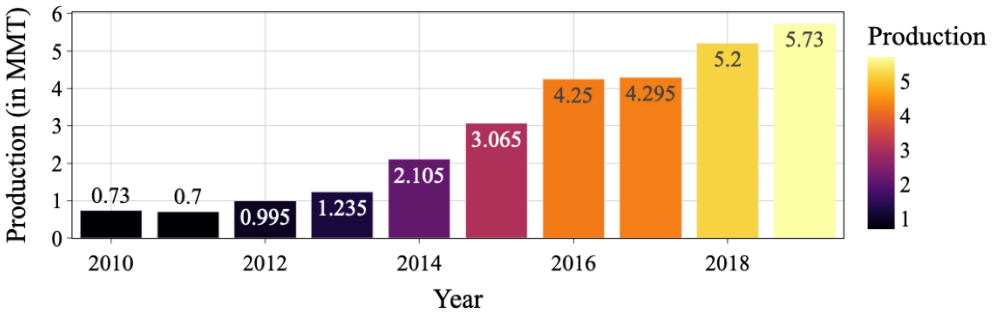

Figure 1. Growth of methanol production in the U.S. in MMT post-decrease in gas prices since 2008 [4].

The first-of-a-kind integration of a nuclear reactor into legacy methanol process plants presents unique challenges. Understanding the dual role of natural gas, both for thermal energy production and as a feedstock for synthetic gas preparation, is the first crucial step. Section 2 provides an overview of a traditional methanol production plant. Section 3 dives into two innovative greenfield pathways for methanol production. The first pathway offers minimal disruption to an existing methanol plant to reduce carbon dioxide emissions by only using hydrogen as a heat source. The second pathway requires more significant modifications to the methanol production process by also using hydrogen as a feedstock to potentially completely eliminate carbon dioxide emissions. Section 4 describes the coupling points and feasibility of integrating advanced nuclear reactors with decarbonized methanol production pathways. Finally, Section 5 presents preliminary thermal design concepts for incorporating advanced nuclear reactor technology into the two proposed decarbonized pathways. Section 6 concludes the report by summarizing the key findings, conclusions, and outlining potential avenues for future research.

2. TRADITIONAL APPROACH TO METHANOL PRODUCTION

This section delves into traditional methanol production with the aid of simplified block flow diagrams. The current approach to methanol production leverages three main subprocesses: synthetic gas preparation, synthetic gas compression and methanol synthesis, and downstream distillation. Figure 2 shows the process steps. The first row summarizes the subprocesses, and the second row offers macro details of subprocess mass and energy flows. The values in Figure 2 were calculated using Aspen Plus for a modern mega-methanol plant with an average output of 10,000 tonnes-per-day (tpd) production capacity.

1. Syngas Preparation: Figure 2 highlights this subprocess in green. It illustrates a combination of the traditional steam-methane reformer (SMR) and a more recent autothermal reformer (ATR) technology for syngas production. Syngas preparation is one of the most energy-intensive processes in natural gas-based methanol production. Focusing on natural gas usage, this subprocess utilizes a total of 7,509 tpd of natural gas (NG).
    a. Natural Gas as Feedstock in Reformers: Roughly 6,200 tpd within the reformers are dedicated to feedstock preparation.
    b. Natural Gas as Fuel in Burners or Furnaces: Around 1,300 tpd are required to power the burners or the furnaces to fulfill heat requirements for synthetic gas production.
2. Syngas Compression and Methanol Synthesis: The second subprocess is delineated in red within Figure 2 consists of two main steps. First, the synthetic gas produced from the combined steam-methane reformer (SMR) and ATR undergoes compression. This step is energy intensive as synthetic gas is preconditioned to a high pressure of 92 bar, requiring 76.5 MWe. Preconditioning of syngas to elevated pressures is crucial because high-pressure conditions are favorable for methanol synthesis. Second, compressed synthetic gas enters the methanol reactor where it undergoes conversion into crude methanol. Methanol synthesis generates heat due to the exothermic nature of the underlying chemical reactions. The heat generated during methanol synthesis and from cooling crude methanol is recovered and is used to preheat incoming synthetic gas and to power downstream distillation columns.
3. Methanol Distillation: Finally, the third subprocess involves distillation of crude methanol, highlighted in blue in Figure 2. It is designed to obtain Grade A methanol of purity 99.95% by weight from the crude methanol. The thermal energy requirements for powering water scrubbers and distillation columns in this subprocess are sourced from the upstream heat recovery system.

For the purposes of this discussion, the key features of methanol production in existing plants are that the required energy is sourced entirely from NG and either on-site electricity production or from grid electricity.

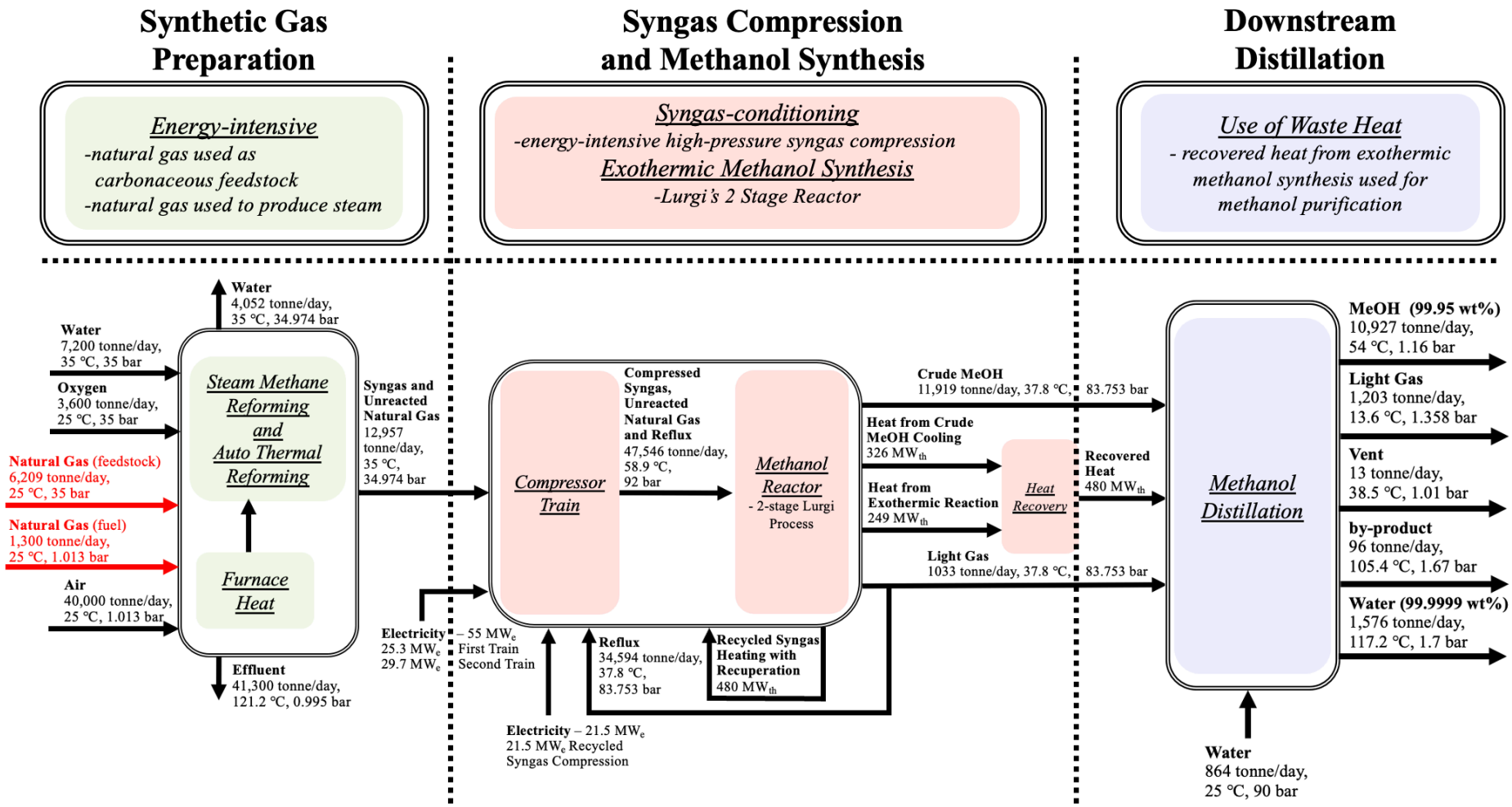

Figure 2. The block flow diagram for a traditional mega-methanol plant using NG as a feedstock and as a fuel for heating.

3. PROPOSED DECARBONIZED METHANOL PRODUCTION PATHWAYS

To support decarbonization efforts by reducing emissions in methanol process plants, NG use as a feedstock and fuel must be mitigated. Complete lifecycle emissions of methanol are over 2.0 kg CO_2/kg MeOH.[5] Building on the 10,000 tpd traditional methanol production plant, two novel decarbonization pathways in methanol production are proposed and modeled using Aspen Plus. To replace NG, an alternative source of energy and feedstock will be needed. Pathway-1 reduces NG use by replacing the heat source in the SMR+ATR with nuclear-generated hydrogen. This hydrogen is used for powering furnaces or burners. Pathway-2 replaces the SMR+ATR entirely via syngas preparation using CO_2 and H_2 with a reverse water gas shift (RWGS) reactor and a Selexol carbon capture process.

3.1 Pathway-1: Use of Hydrogen to Replace Natural Gas for Powering Furnaces

This section details a decarbonization strategy that replaces the consumption of 1,300 tonnes of NG per day in burners (highlighted in red text under syngas preparation within Figure 2). The proposed replacement fuel is hydrogen gas. This hydrogen would be produced via high-temperature steam electrolysis (HTSE) and then integrated as furnace heat for a SMR as shown in Figure 3.

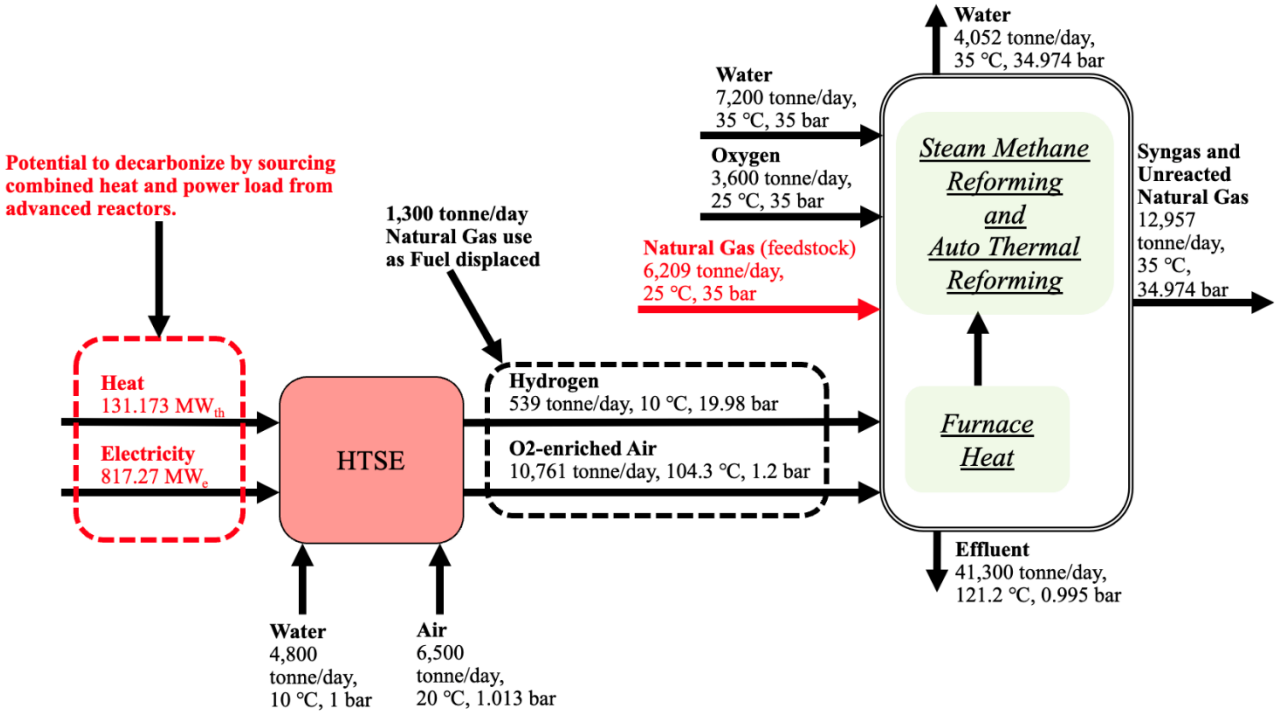

Figure 3. Replacement of NG as a fuel with hydrogen to power burners or furnaces providing heat to two-stage reformers.

3.1.1 H_2 Preparation: High-Temperature Steam Electrolysis

In this process, HTSE is used to produce hydrogen. Unlike ordinary water electrolysis that directly converts liquid water into gaseous hydrogen and oxygen using electricity only, HTSE requires steam to be introduced to the electrolyzer. This reduces the electrical load by harnessing thermal energy equivalent to the heat of vaporization. Depending on exact operating temperature conditions and corresponding sensible heat of H_2O, approximately 15% of electricity for direct electrolysis can be substituted by thermal energy from a heat source. The thermal energy demand may be reduced due to the Joule heating of an electrolysis cell.

[Direct electrolysis] $$H_2O_{(l)} \rightarrow H_{2,(g)} + 0.5\ O_{2,(g)} \qquad \Delta H^{\circ}_{rxn@298K} = 285.8 \frac{\text{kJ}}{\text{mol}} \tag{1}$$

[HTSE] $$H_2O_{(l)} \rightarrow H_2O_{(g)} \qquad \Delta H^{\circ}_{@298K} = 44.0 \frac{\text{kJ}}{\text{mol}} \tag{2}$$

$$H_2O_{(g)} \rightarrow H_{2,(g)} + 0.5\ O_{2,(g)} \qquad \Delta H^{\circ}_{@298K} = 241.8 \frac{\text{kJ}}{\text{mol}} \tag{3}$$

Solid oxide electrolysis cells (SOEC) are electrolysis units used for HTSE. High-temperature steam (750–850°C) is introduced to the cathode of the electrolyzer and dissociated into a hydrogen molecule and an oxygen ion at the cathode. Oxygen ions are diffused through the solid oxide electrolyte and converted into oxygen molecules at the anode. Maintaining a high temperature is preferred when integrating electrolysis with nuclear plants both to increase reaction kinetics and to reduce the electrical (and more expensive) energy requirement [6]. The efficiency of converting H_2O to H_2 can be as high as 90% for utilization rate of 80% H_2O per pass in the SOEC. H_2 product flows out of the SOEC with unreacted H_2O; thus, a separation process is necessary. Operating temperature and pressure at the SOEC are determined as 800°C and 5 bar, respectively [7].[a]

The HTSE model is built in Aspen Plus, extending a previous model constructed at INL[7]. Figure 4 presents the process flow diagram of the HTSE process to produce H_2 at 539 tpd. The pre-treated water enters the HTSE facility and is first preheated via heat recovery by a product downstream of the SOEC (**E-2**, **E-3** on Figure 4). Then, vaporization of feedwater occurs in a heat exchanger using heat from a nuclear power plant (NPP) (**E-4**), in which the water at 11.11 bar is depressurized to 5.4 bar and fully vaporized. The boiling temperature of water is 151.6°C and 184.3°C at pressure of 5 and 11 bar, respectively. The outlet temperature of a heat exchanger connected with an NPP is specified as 200°C. Then, steam enters the SOEC (**E-9**). To reach the operating temperature of SOEC (800°C), additional heat is recuperated downstream from the NPP heat exchanger via SOEC product streams (**E-5** and **E-7**). Subsequently an electric ceramic heater is leveraged to heat the feedstock to operating temperature (**E-8**). The hydrogen steam mixture is produced at the cathode of SOEC. To maintain a reducing environment on the cathode side and prevent premature material degradation, one-eighth of the H_2-H_2O mixture after the SOEC are recycled back to the SOEC (**W15B**). Hydrogen must be purified and pressurized before use. Water is condensed and separated out from the hydrogen (**E-11, E-14, E-17**) by increasing pressure (**E-12, E-15**) and decreasing temperature (**E-10, E-13, E-16**). High--purity (99.9 wt%) hydrogen can be obtained at the end of this process (**W24**) and stored at 20 bar.

[a] Precise operating temperatures and pressures within a given SOEC stack will be dependent on the specifics of the SOEC design and vendor. The cited values are taken as representative ones for the purposes of this written report. The authors do not anticipate that the overarching conclusions and results of this report would be different with slightly different HTSE conditions.

Oxygen is generated on the anode side of the SOEC stack. As a high concentration of O_2 at high temperatures may damage the system, heated air is introduced to the outlet of the SOEC to sweep out the oxygen gas produced. To minimize the temperature gradient at the anode, air is preheated by anode product streams in heat exchangers (**E-20**, **E-22**) and via electric heater (**E--21**) to 800°C. In the end, O_2-rich air is released. However, before its release, a turbine (**E-23**) recuperates energy in the form of electricity.

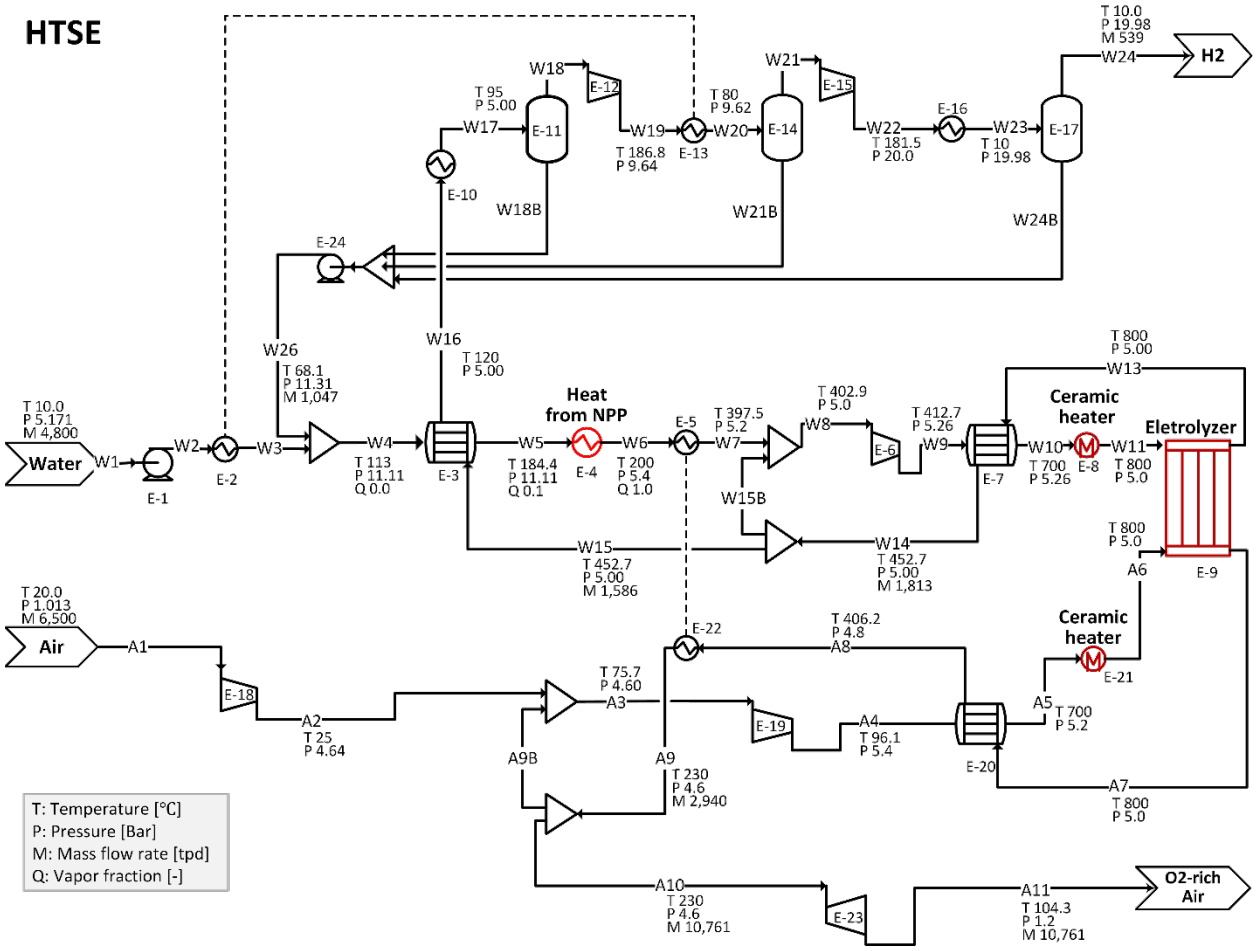

Figure 4. Process flow diagram of HTSE as scaled for Pathway-1.

The thermal energy and electricity requirements of the HTSE unit for each process in the planned pathways are listed in Table 1. As noted above, in Pathway-1 hydrogen is burned as a fuel, whereas in Pathway-2, hydrogen is used separately in RWGS and preconditioning processes. The energy required for HTSE has a linear relation to the hydrogen production. Based on the Aspen Plus model analysis, the heat exchanger (**E-4**), in which water is vaporized, is the only unit that can harness thermal energy from an NPP. Heat must be delivered at temperature higher than 200°C. The energy used for "processed" water (demineralizing, pumping, etc.) is not considered in this calculation.

Table 1. Energy requirement on each unit for HTSE process with different purpose.

Unit Name in Figure 4	Unit Type	Energy Type	Energy Requirement [MW]		
			Pathway-1: Hydrogen Fuel Burner	Pathway-2: RWGS	Pathway-2: Pre-conditioning
E-9	Electrolyzer	Electricity	765.51	877.96	426.19
E-4	Water vaporization unit coupled with NPP	Heat	131.17	144.48	71.12
E-8	Ceramic heater for Water	Electricity	17.40	19.94	9.68
E-21	Ceramic heater for carrier gas	Electricity	11.45	11.87	5.76
E-18	Compressor for carrier gas	Electricity	15.08	15.45	7.51
E-6	Compressor for steam	Electricity	1.53	1.76	0.86
E-12	Compressor for H_2 separation	Electricity	10.06	11.58	5.65
E-15	Compressor for H_2 separation	Electricity	9.68	11.11	5.40
E-19	Compressor for carrier gas	Electricity	2.05	2.13	1.03
E-23	Turbine for carrier gas	Electricity	-15.54	-16.64	-8.08
E-1	Pump	Electricity	0.044	0.08	0.03
E-24	Pump	Electricity	0.010	0.01	0.004
Total		Electricity	817.27	935.25	454.03
		Heat	131.17	144.48	71.12
The amount of hydrogen produced [tpd]			539	618	300

3.1.2 Hydrogen Furnace for Steam-Methane Reformer

In Pathway-1 hydrogen replaces methane as fuel in the burner to decarbonize the furnace operation. Figure 5 shows the process flow diagram of Pathway-1 using a hydrogen-fired furnace. This differs from burning NG within the furnace, as seen in the inset of Figure 5. Instead, the HTSE module (**B-13**) is added to the reference methanol synthesis process model to produce and supply hydrogen into the furnace [8]. Table 2 contrasts the heat and fuel required at the furnace for SMR in the traditional design and for Pathway-1. The reference methanol model requires 688.40 MWth of heat in the SMR process, which is provided by burning 1,300 tpd of methane (equivalent to 747.36 MW). NG, with constituents as 95, 3, and 2 mole % of methane, ethane, and propane, respectively, has a lower heating value of 49.69 MJ/kg, whereas H_2 has a lower heating value of 120 MJ/kg. To match the heat obtained from burning NG, 539 tpd of hydrogen must be consumed. The heat and electricity required for HTSE to produce 539 tpd of hydrogen is 131.17 MWth and 817.27 MWe.

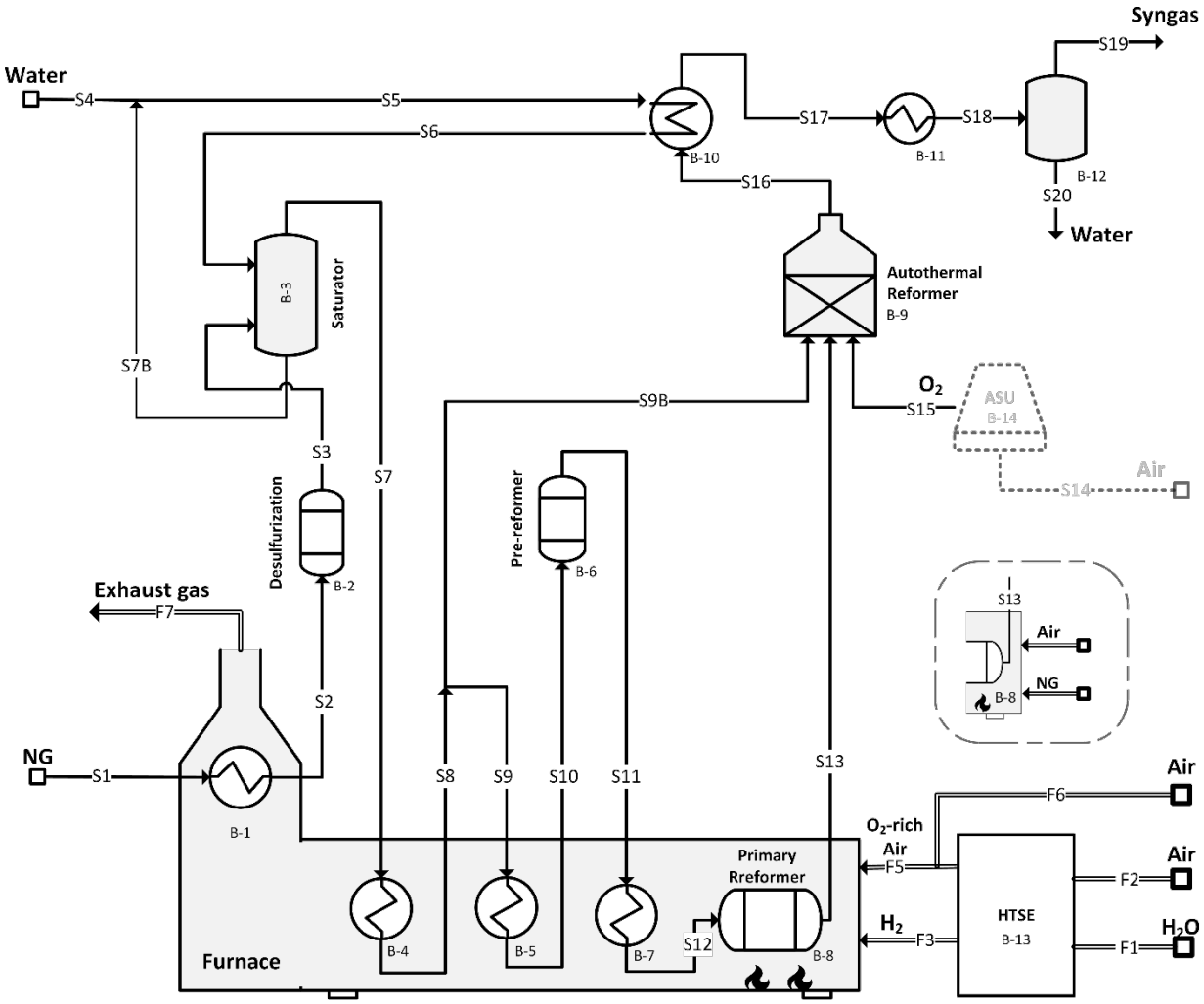

Figure 5. Process flow diagram for SMR/ATR process with the hydrogen-burning furnace.

Table 2. Energy requirement and amount of energy converted with HTSE at the SMR furnace.

	Methane	H_2	Efficiency [%]
The amount of the heat transferred from the furnace to SMR/ATR process [MW] / [GJ/tonne MeOH]	688.40 (5.44)		72.58
Energy contained in the fuel [MW] / [GJ/tonne MeOH]	748.61 (5.92)		78.93
The corresponding amount of fuel [tpd]	1,300	539	—
Energy requirement for HTSE process [MW]	—	Heat: 131.17 (1.04) Electricity: 817.26 (6.46)	100

In addition to fuel, air must also be supplied. Excessive air introduced to the furnace works not only as the source of O_2 but also as the damper of rapid temperature increment of the flue gas. If only the exact amount of air needed for complete combustion is supplied, the temperature after the primary SMR reactor (**B-8**) might increase to the degree where nitrogen compounds synthesize, and the furnace could be damaged. The temperature of the primary reformer and corresponding portion within the furnace is estimated as 961.7℃. It is important to keep the combustion temperature below approximately 1200℃ to avoid the formation of polluting nitrous oxides. For the furnace, both O_2-rich air from the HTSE of 10,761 tpd and extra air of 30,000 tpd are supplied. An ATR needs oxygen supplied from an air separation unit. It may be possible to use O_2-rich air, such as from the HTSE anode exhaust, to produce high-purity O_2 for ATR but the current model does not consider it. It is assumed that pure O_2 is introduced to the ATR.

The main purpose of the H_2 furnace is to reduce CO_2 emission from burning NG. Table 3 compares CO_2 emissions from a traditional methanol synthesis process in which NG is burned with CO_2 emissions from Pathway-1 in which hydrogen is burned. CO_2 emissions at the furnace can be completely removed by substituting CH_4 with H_2. However, CO_2 emission from the entire process still exists. Some CH_4 remains after SMR, and some CO and CO_2 remain after methanol synthesis. These unreacted reactant gases, named light gas, are separated and released into the atmosphere through the distillation process. These fugitive emissions accounts for the main source of greenhouse gas (GHG) released during the hydrogen-burning SMR process. Approximately 10% of CH_4 remains and exits as light gas from SMR/ATR methanol synthesis. Methane is 30 times more potent than CO_2 as a GHG, so burning it in a flare tower reduces climate impacts. Methane can also be an alternative source of fuel in the furnace but that is not considered in this calculation. In short, 62.8% of scope-1 [b]CO_2 emissions can be reduced by substituting the NG fuel in the furnace. The Pathway-1 still has a high amount of lifecycle CO_2 emissions considering that methane is still used as a feedstock for producing methanol. Lifecycle CO_2 reduction is estimated at 17%, assuming that synthesized methanol is entirely consumed in a manner that re-emits the C atom in the form of CO_2. Considering the potential emissions associated with the end use of the product methanol is outside the scope of this report.

[b] "The GHG Protocol Corporate Standard classifies a company's GHG emissions into three 'scopes'. Scope 1 emissions are direct emissions from owned or controlled sources. Scope 2 emissions are indirect emissions from the generation of purchased energy. Scope 3 emissions are all indirect emissions (not included in scope 2) that occur in the value chain of the reporting company, including both upstream and downstream emissions."[9]

Table 3. CO_2 emission from a traditional methanol synthesis process burning CH_4 and H_2.

Scope	Furnace with CH_4 Burning [kg CO_2 eq. / kg MeOH]	Furnace with H_2 Burning [kg CO_2 eq. / kg MeOH]
Furnace (Ⓐ)	0.329	0
Flare tower after burning unreacted feedstock and byproduct (light gas) (Ⓑ)	0.195	0.195
CO_2 contained in Methanol product (Ⓒ)	1.375	1.375
CO_2 released as feedstock emissions, drilling, and transportation (Ⓓ)	not considered	not considered
CO2 emission from the facility (Ⓐ + Ⓑ)	0.524	0.195
Lifecycle emission total (Ⓐ + Ⓑ + Ⓒ)	1.899	1.570

3.2 Pathway-2: Use of Hydrogen and Carbon-Dioxide to Eliminate Natural Gas Requirement for Feedstock Preparation

In this section, a more comprehensive strategy is described to eliminate the entire 7,209 tpd of NG that is consumed in a traditional methanol plant. The proposed pathway entails a radical modification to the syngas preparation: replacement of the SMR and ATR with an HTSE process for hydrogen preparation and introducing an RWGS process for CO preparation from an atmospheric source of CO_2. Overall, syngas feedstock is changed from CH_4 to H_2O and CO_2, enabling a near-zero CO_2 lifecycle emission. The carbon dioxide for RWGS is assumed to be available as a stream from a separate industrial process that would otherwise emit the carbon dioxide to the atmosphere or from an atmospheric direct air capture system. The temperature in the RWGS reactor is 600°C, and the amount of heat required is less than for SMR. An alternative method to deliver heat can be chosen instead of a furnace that consumes CH_4. The Selexol process is added to remove and separate unreacted CO_2 from syngas to separate and remove syngas constituents before methanol synthesis. Figure 6 shows the block flow diagram of RWGS-Selexol process configuration as a substitution for the SMR/ATR process. All values are estimated from the Aspen Plus model.

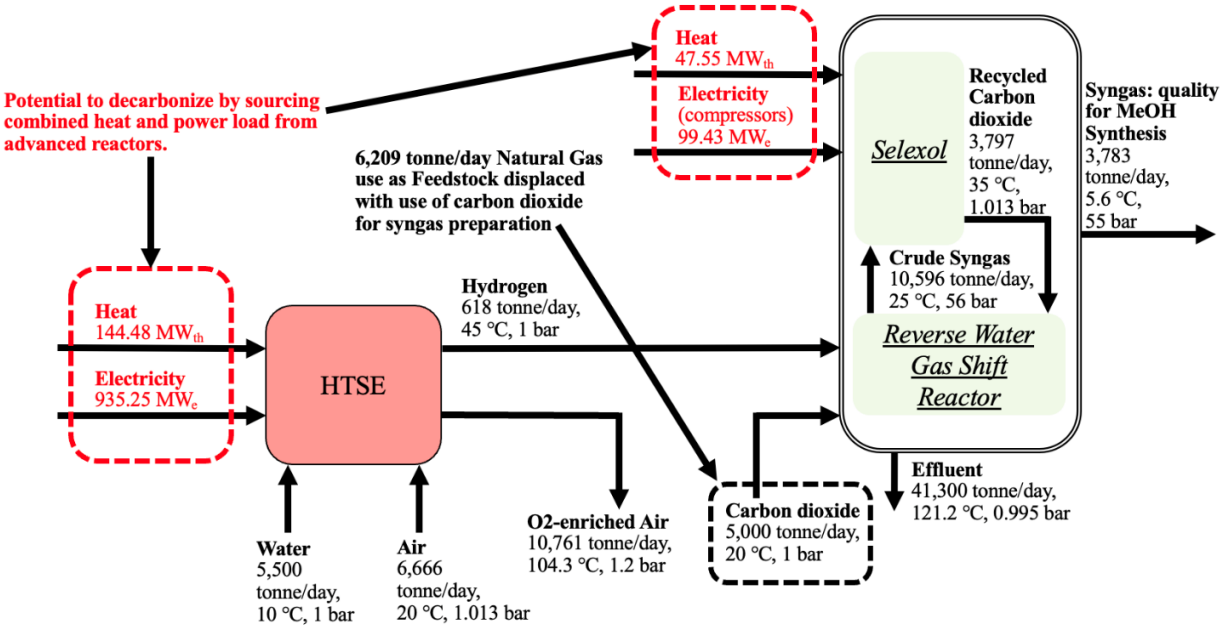

Figure 6. 100% replacement of NG as both a fuel and a feedstock with syngas preparation using hydrogen and carbon dioxide using an RWGS-Selexol process configuration.

3.2.1 CO Preparation: Reverse Water Gas Shift Reaction

This section describes the Pathway-2 process focused on CO preparation. The RWGS and Selexol processes are explained. Hydrogen preparation by HTSE with an NPP was previously discussed in Section 3.1.1. To create syngas, H_2 needs to be mixed with CO. Given the HTSE source for H_2, a CO source must be identified. CO_2 reduction to CO occurs with hydrogen via RWGS reaction as shown in Equation (4). This process consumes CO_2 to generate CO. The RWGS reactor operates endothermically at 600°C, which is significantly cooler than the operating temperature of an SMR (approximately 850°C), potentially enabling the use of an alternative heat source for the furnace. In designing an RWGS reactor, competing side reactions of CO reduction with hydrogen, called CO_2 methanation, must be accounted for. Reaction equations and their reaction enthalpy for both reactions are written below.

RWGS: $$CO_2 + H_2 \leftrightarrow CO + H_2O \qquad \Delta H_{0.298} = 41kJ/mol \tag{4}$$

CO_2 methanation: $$CO_2 + 4H_2 \leftrightarrow CH_4 + 2H_2O \qquad \Delta H_{0.298} = -165kJ/mol \tag{5}$$

The kinetic preference for each reaction depends on temperature, pressure, and catalyst. An RWGS reaction is an endothermic reaction, whereas a CO_2 methanation reaction is an exothermic reaction. RWGS is driven preferentially at high-temperature conditions while CO_2 methanation occurs with greater frequency at low temperature. The net stoichiometric coefficient of an RWGS reaction is zero while CO_2 methanation has a negative value. This indicates that the RWGS reaction does not depend on pressure, but forward reaction of CO_2 methanation is promoted as pressure increases. Catalyst selection does not change the thermodynamic equilibrium but can change the reaction rate for each reaction separately. In a practical situation, reaction yield can be controlled through reactor sizing. Selective catalyst must be chosen carefully to suppress the methanization reaction rate and to expedite the RWGS reaction [10]. Gonzalez-Castano et al. investigated and summarized CO_2 conversion and CO selectivity for a RWGS reaction. Traditional metallic catalysts, alkali addition catalysts, and transition metal carbide/sulfide catalysts are investigated. In addition, the composition ratio of the catalyst can affect selectivity. Zhang et al. found that the selectivity of Mo-Ni bimetallic catalyst can be switched in two extreme cases based on the Mo-Ni ratio [11]. This study chose a catalyst model tested by Kim et al. [12]. An experiment was conducted for RWGS reaction with a BZYZ catalyst at a temperature of 600℃ and atmospheric pressure, yielding CO_2 conversion and CO selectivity as 37.5% and 97%, respectively.

With the BZYZ catalyst under specified operating conditions, CO_2 of 62.5% remains unreacted, and thus is the majority component downstream. Similar CO_2 conversion was found based on thermodynamic equilibrium estimation. High concentration of CO_2 is known to attenuate performance of methanol (MeOH) production (Bussche and Froment) [13]; so CO_2 needs to be removed from syngas and refluxed back as feedstock of the RWGS reaction. The Selexol process, which is a mature and well-adopted process, is selected to capture unreacted CO_2. Doctor et al. developed a CO_2 capture process that is coupled with integrated gasification and combined cycle power generation using Aspen Plus [14]. In this study, a Selexol process is used. A dimethyl ethers of polyethylene glycols (DEPG) solvent selectively dissolves CO_2 and H_2S over other gases such as H_2 or CO, enabling CO_2 separation. Captured CO_2 is separated from the DEPG solvent and recycled to the RWGS reactor. It is calculated that approximately 90% of CO_2 can be dissolved and captured through the Selexol process, which is enough capture performance for methanol production.

The bottom portion of Figure 7 shows the process flow diagram of the RWGS + Selexol process model. The model in Figure 7 begins by assuming hydrogen produced from HTSE and a CO_2 source is captured and transported from other chemical facilities. CO_2 is also captured and recycled from the Selexol process. This raw material stream is preheated by a heat recuperation heat exchanger (**E-2**) and an electric ceramic heater (**E-3**) up to 600℃. The feedstock is depressurized to 1.013 bar. An “Rstoic” reactor (**E-4**) specifies the yield of two competing reactions (RWGS and CO_2 methanation) as 36% and 1%, respectively based on the experimental result [12]. The operating temperature is designed to be maintained at 600℃, and the endothermic reaction heat is supplied from an outside heat source. Operating pressure of the reactor is specified as atmospheric pressure based on the reference data. The bottom portion of Figure 7 shows the process flow diagram of the RWGS + Selexol process model. The model begins by assuming hydrogen produced from HTSE and a CO_2 source captured and transported from other chemical facilities. CO_2 is also captured and recycled from the Selexol process. This raw material stream is preheated by a heat recuperation heat exchanger (**E-2**) and an electric ceramic heater (**E-3**) up to 600℃. The operating temperature is designed to be maintained at 600℃, and the endothermic reaction heat is supplied from an outside heat source. The operating pressure of the reactor is specified as atmospheric pressure based on the reference data.

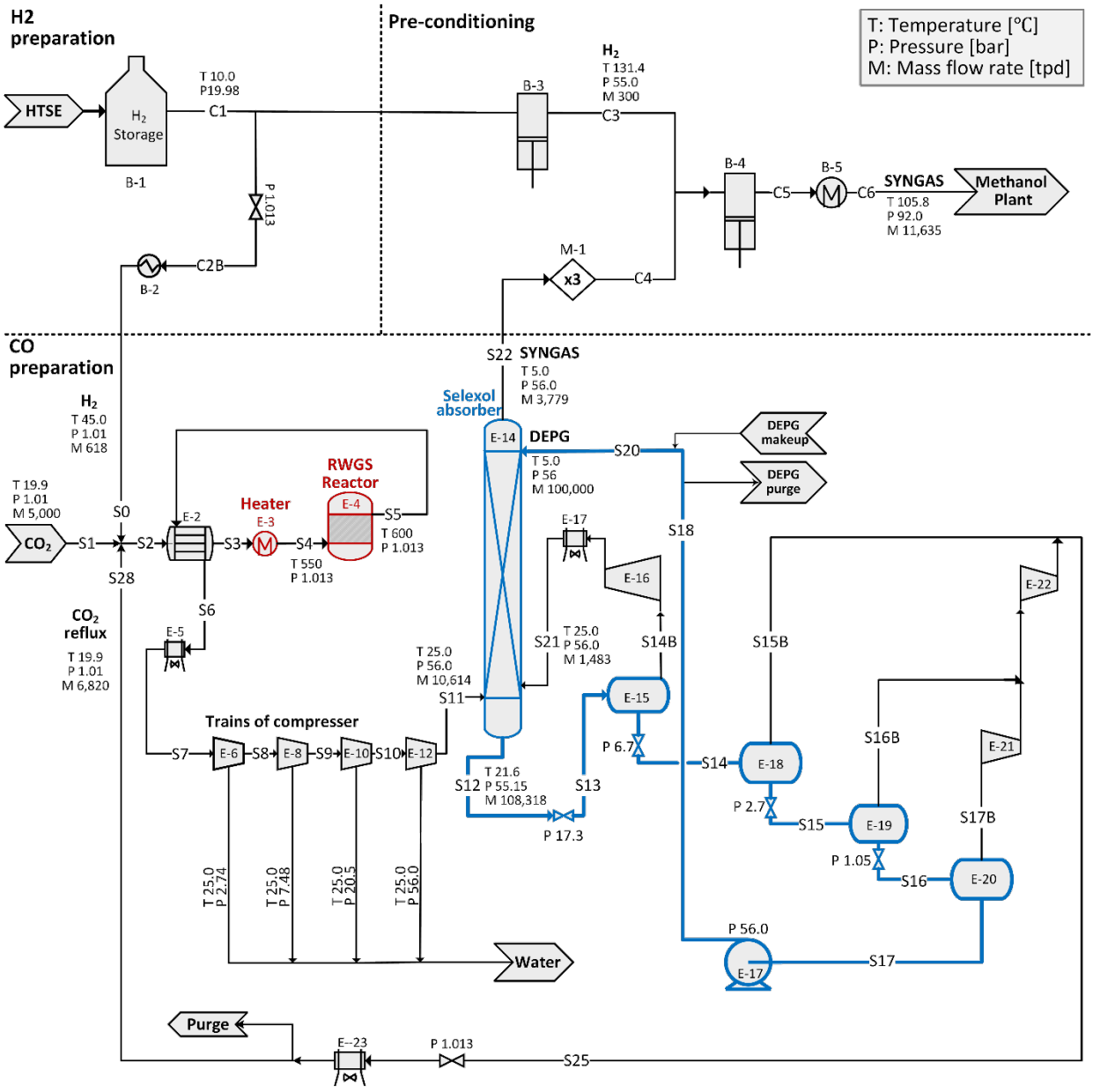

Figure 7. Process flow diagram for RWGS process and preconditioning of syngas.

After the RWGS reactor, the crude syngas stream is compressed to 56 bar through four compressor stages (**E-6, E-8, E-10, E-12**) before being introduced into the absorber tower. The flow is cooled down to 25°C after each compressor stage. The streams colored blue on Figure 7 demonstrates the DEPG solvent circulation loop, referred to as the Selexol process. The absorber tower (**E-14**), which has a diameter of 17 feet and a height of 108 feet, has 36 stages, packed with 50-mm metal packing. Table 4 shows the stream information for all the inlets and outlets of the Selexol absorber. Liquid DEPG solvent with temperature of 5°C is introduced to the top of the absorber tower while CO_2-rich syngas is introduced at the bottom of the tower. The volumetric flow rate of the solvent is estimated as 2,273 cubic feet per minute (cfm). The solvent physically dissolves the acid gases (CO_2 and H_2S) from the feed gas, yielding 91.79% CO_2 capture performance. The CO_2-lean syngas coming from the top of the absorber does not have to be of high purity. Rather, some CO_2 in syngas reportedly improves methanol synthesis performance. CO_2- rich solvent from the bottom of the tower goes to the sump tank (**E-15**) at 17.3 bar in which light gas can escape from the liquid. The less soluble gas released from the sump tank is pressurized to 56 bar and recycled to the 34th stage of the tower. Solvent that removed light gas goes to flash tanks 1, 2 and 3 in series (**E-18, E-19, and E-20**). CO_2 is released in the tanks from the solvent by reducing the pressure to 6.7, 2.5, and 1.05 bar, respectively. Re-captured high-purity CO_2 is refluxed back to the beginning of the process, and regenerated solvent is re-pressurized by the pump (**E-17**) and recycled back to the absorber. In a nutshell, under current single process specification, CO_2 of 5,000 tpd and hydrogen of 618 tpd are introduced to RWGS + Selexol process, generating 3,779 tpd of syngas. Note that the amount of syngas from single RWGS + Selexol process is not large enough for the reference methanol plant model, and its composition is not best for methanol synthesis. Further steps are required as explained in the next section.

Table 4. Stream result at Selexol absorber.

	S11 [In]	S21 [In]	S20 [In]	S22 [Out]	S12 [Out]
Stream	CO_2-rich Syngas	Light Gas Reflux	DEPG Solvent	CO_2-lean Syngas	CO_2-rich Solvent
Stage	36 (bottom)	35	1 (top)	1	36
Phase	Gas	Gas	Liquid	Gas	Liquid
Temperature [°C]	25.00	25.00	5.00	5.55	21.63
Pressure [Bar]	56.00	56.00	55.00	55.00	55.15
Mass flowrate [tpd]	10,613.83	1,482.52	100,000.00	3,778.51	108,317.84
Volume flowrate [cfm]	4,949.28	346.34	2,273.43	3311.15	2,531.93
Component mass flowrate [tpd]					
H_2	400.492	9.09	1.82E-06	399.71	9.87
CO	2,749.02	119.40	4.60E-04	2,727.23	141.20
CO_2	7,404.72	1,350.04	715.20	608.10	8,861.86
H_2O	15.24	0.33	1,095.33	0.62	1,110.28
CH_4	44.35	3.66	3.45E-4	42.85	5.16
DEPG	0.00	4.44E-04	98,189.47	2.44E-04	98,189.47
CO_2 removal efficiency compared with S11 [%]				91.79	—

The energy requirement for each unit in a single RWGS + Selexol process are listed in Table 5. Energy used for the HTSE system accounts for 88% of the entire energy requirement of new syngas preparation. The HTSE needs 144.48 MWth and 935.27 MWe, whereas the energy used for the RWGS and the Selexol process itself needs 47.55 MWth and 112.86 Mwe. The preheater (**E-3**) and RWGS reactor (**E4**), red-colored in Figure 7, are the units that require 600℃ heat delivery while the pump and compressors require electricity.

Table 5. Energy requirement on each unit for RWGS + Selexol process.

Unit Name on Figure 7	Unit Type	Energy Type	Energy Requirement	
			Single RWGS + Selexol [MW]	Temperature [℃]
HTSE1	H_2 production for RWGS	Heat	144.48	200
		Electricity	935.25	—
E-4	RWGS chemical reactor	Heat	34.13	600
E-3	Heater	Heat	13.42	600
E-6,8,10,12	Multi-stage compressor	Electricity	86.69	—
E-17	Pump for solvent recirculation	Electricity	7.30	—
E-16	Compressor for CO_2 before absorbing tower	Electricity	1.77	—
E-21	Compressor for CO_2 recirculation	Electricity	0.86	—
E-22	Compressor for CO_2 recirculation	Electricity	2.82	—

3.2.2 Elimination of Natural Gas Usage using Reverse Water Gas Shift

Pathway-2 is designed to eliminate the entire usage of NG from the traditional methanol process. SMR syngas preparation (green-colored portion in Figure 2) is entirely substituted by HTSE and the RWGS process as mentioned in previous sections. Methanol synthesis and the distillation subsection are unchanged relative to the reference methanol model based on the Lurgi process.

Syngas made by a novel process should thus have a similar composition of syngas by traditional process, and thus preconditioned to the same conditions before the methanol synthesis process. The amount of syngas used in the reference methanol model is 12,957 tpd, while the amount of syngas produced using the RWGS + Selexol configuration process mentioned in previous section is 3,779 tpd. Thus, three sets of RWGS + Selexol units are required to match the amount of syngas needed. Additionally, Syngas produced from RWGS + Selexol configuration process has H_2, CO, and CO_2 mole fractions estimated as 0.635, 0.311, and 0.044, respectively. Extra hydrogen needs to be added to achieve the best condition for methanol synthesis with H_2, CO, and CO_2 mole fractions of 0.70, 0.27, and 0.03, respectively [13].

The energy requirement for each unit is estimated and summarized in Table 6. Three sets of RWGS + Selexol processes are installed. HTSE requirements are split between the syngas preconditioning (300 tpd) and H_2 preparation. The modified syngas is preconditioned to 105.8℃ and 92 bar.

Table 6. Energy requirement of each unit for entire substitution of SMR.

H_2 and CO preparation [MW]			
HTSE1	H_2 production (619 tpd each) for RWGS	Heat	433.44 (144.48 × 3)
		Electricity	2805.81 (935.27 × 3)
RWGS + Selexol	CO production	Heat	142.65 (47.55 × 3)
		Electricity	338.58 (112.86 × 3)
Syngas preconditioning			
HTSE2	Extra H_2 production (300 tpd) for MeOH synthesis	Heat	71.12
		Electricity	454.04
B-3	Compressor for extra H_2 before MeOH synthesis	Electricity	6.0
B-4	Compressor for syngas before MeOH synthesis	Electricity	22.2
B-5	Heater for syngas before MeOH synthesis	Electricity	9.1

Through Pathway-2, 11,635 tpd of syngas with H_2, CO, and CO_2 mole fractions of 0.685, 0.269, and 0.038, respectively, are prepared and introduced to the methanol synthesis and distillation processes. This results in high-purity methanol production of 10,299 tpd. As investigated in the reference methanol production model in a previous INL report, the energy required for the distillation process can be covered by the heat produced from the exothermic methanol synthesis reaction [8]. No further external energy is required for those two subprocesses. The amount of 600°C required at the preheater and the RWGS reactor are estimated as 142.65 MWth. This needs to be supplied from either a high temperature nuclear reactor or a supplementary furnace that leverages byproducts isolated from the distillation tower.

In the end, the total energy requirement for Pathway-2 is estimated as 35.59 GJ/tonne MeOH produced. This is similar to the amount of energy used in traditional methanol synthesis (34.15 GJ/tonne MeOH). However, as listed in Table 8, the emission of CO_2 gas can be reduced to 0.083 kg CO_2/kg MeOH, an 84% reduction compared with the reference methanol production model. Furthermore, considering the potential atmospheric CO_2 consumption within Pathway-2, the CO_2 lifecycle emission can become zero.

Table 7. Energy requirement for methanol synthesis via Pathway-2.

Process	Thermal [MW] / [GJ/tonne]	Electricity [MW] / [GJ/tonne]
H_2 production (HTSE)	504.56 (4.23) @ 200℃	3,259.85 (27.34)
CO production (RWGS)	142.66 (1.20) @ 600℃	298.32 (2.50)
Preconditioning	0 (0)	37.3 (0.32)
Methanol synthesis + distillation	0 (0)	0 (0)
Total	647.22 (5.43)	3,595.47 (30.16)

Table 8. CO_2 emission from traditional methanol synthesis process with CH_4 and H_2 burning.

Emission Part	SMR/ATR process with furnace with CH_4 burning [kg CO_2 eq. / kg MeOH]	Zero usage of methane RWGS + HTSE [kg CO_2 eq. / kg MeOH]
Furnace (Ⓐ)	0.329	0
Flare tower after burning unreacted feedstock and byproduct (light gas) (Ⓑ)	0.195	0.083
CO_2 contained in Methanol product (Ⓒ)	1.375	1.375
CO_2 released at feedstock emissions, drilling and transportation (Ⓓ)	not considered	not considered
CO_2 utilization (consumed) (Ⓔ)	0	1.458
CO2 emission from the facility (Ⓐ + Ⓑ)	0.524	0.083
Lifecycle emission total (Ⓐ + Ⓑ + Ⓒ − Ⓔ)	1.899	0.000

4. POTENTIAL OPPORTUNITIES TO INTEGRATE ADVANCED REACTORS

This section will describe the NPP that will be connected to the methanol facility and how heat and electricity will be prepared. As discussed in Section 3, the primary opportunity for integrating nuclear energy is via HTSE. As such, the analysis in this section will focus on designing a combined heat and power (CHP) system that can satisfy the requirements outlined in the previous section.

4.1 Reactor Technologies

Two reactor designs are analyzed in this report: the NuScale VOYGR LWR and X-energy's Xe-100 HTGR. Aspen HYSYS was used to develop the balance of plant (BOP) and thermal extraction models. The steam header conditions for both reactor technologies are seen in Table 9.

Table 9. Steam header conditions for both reactor designs.

	Temperature (°C)	Pressure (bar)	Mass Flow Rate (kg/s)
NuScale VOYGR LWR	283	32.8	102.8
X-Energy Xe-100 HTGR	565.5	161.4	77.99

Currently, the NuScale US-600 design, with a capacity of 180 MWth and 50 MWe, is the only small modular reactor that has obtained full design approval from the Nuclear Regulatory Commission. NuScale has released a new design, the US-460 design, which will uprate the US-600 design to 250 MWth and 77 MWe without significantly altering the design. The US-460 design has six 77 MWe NuScale power modules (NPMs). The NuScale VOYGR module generates steam at 283°C and 32.8 bar at a mass flow rate of 102.8 kg/s. A Rankine cycle is used, which has a nominal system efficiency without any industrial extractions of 30.8%. X-energy's Xe-100 design is designed to produce 200 MWth and 80 MWe using a Rankine cycle with a claimed efficiency of nearly 40%. The steam header conditions are 565°C and 160 bar, and the mass flow rate is 77.99 kg/s.

The required temperature and pressure for the vaporization unit for HTSE is about 205°C and 5.4 bar per Figure 4.

4.2 Pathway-1: Hydrogen Fuel Burners

4.2.1 Energy Requirement

For the Pathway-1 methanol synthesis process, 10,927 tpd of MeOH is produced. In Pathway-1, H_2 is used as fuel instead of natural gas for the SMR furnace, 817.27 MWe of electrical energy and 131.17 MWth of process steam at a temperature of 200°C is needed for the HTSE process that produces 539 tpd of hydrogen.

4.2.2 Integration with an Advanced Light-Water Reactor

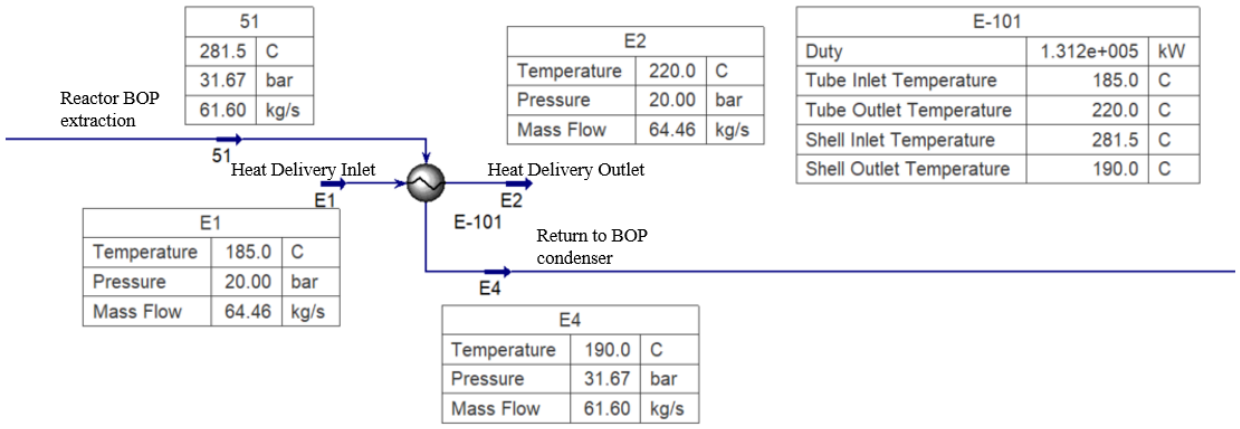

Figure 8. Heat exchanger balance for the LWR on the NPP side supplying steam to be transported to the HTSE.

To produce 539 tonnes-H_2/day (6.238 kg/s), the duty for the heat exchanger needs to be 131.2 MWth, including delivery line losses. The necessary heat is obtained by extracting steam from the main steam header upstream of the turbines. The heat source for the HTSE water vaporization unit must be sufficiently above the boiling temperature for the heat exchange to occur efficiently. While the HTSE unit model uses a lower pressure, the heat transfer fluid is assumed to be steam at 20 bar and 220°C to account for losses in the delivery line between the NPP and HTSE.

Considering these requirements, steam was taken at 61.6 kg/s from the steam header at 281.5°C and 31.67 bar to be used in the heat exchanger to heat the transport steam from a temperature of 185°C to 220°C as indicated in Figure 8. The transport steam moves through the heat exchanger at a mass flow rate of 64.46 kg/s. The condensate is reintegrated into the nominal nuclear steam cycle at the steam generator inlet (using a small amount of pumping to account for pressure drop in the extraction line and HTSE heat exchanger) after being cooled down to the nominal feedwater temperature (shedding 18.5 MWt to the environment). The CHP NPM is expected to generate 36.6 MWe in addition to the HTSE heat assuming the turbine island scales well to produce electricity at 30.8% efficiency (the same as the nominal efficiency value). Overall, this CHP module will operate with 67% efficiency.

4.2.3 Integration with a High-Temperature Gas Reactor

Similar to the case with LWR, a heat duty of 131.2 MWth is needed to produce 539 tonne- H_2/day (6.238 kg/s). Similarly, the inlet temperature of the water vaporization unit must be above 200°C. For the case of a high temperature gas reactor, steam is bypassed from the steam header into a backpressure turbine to generate electricity while reducing the steam conditions to 274.7°C and 22.61 bar. These conditions are sufficient to produce steam for the HTSE unit at 20 bar, raising the temperature from 185°C to 220°C. The mass flow rate of the transfer fluid is 64.47 kg/s. Most of the condensate is sent directly to the feedwater train with 2 kg/s being split and recirculated into the bypass stream going to the HTSE heat exchanger. This recirculation allows for some de-superheating in the steam bypass line and reduces the heat exchanger size. A pump is needed in the system to account for pressure loss in the heat exchanger and in the piping lines and thus the decision of recirculating steam is based on economic considerations, rather than thermodynamic benefits. The condensate outlet of the heat exchanger is at a temperature of 188.8°C and a pressure of 22.51 bar. The HTGR cycle is shown in Figure 9. Figure 10 illustrates that the 61 kg/s sent back to the BOP is utilized with 0.26 kg/s going into a mixer before the feedwater heaters, and 60.74 kg/s is mixed in between the feedwater heaters.

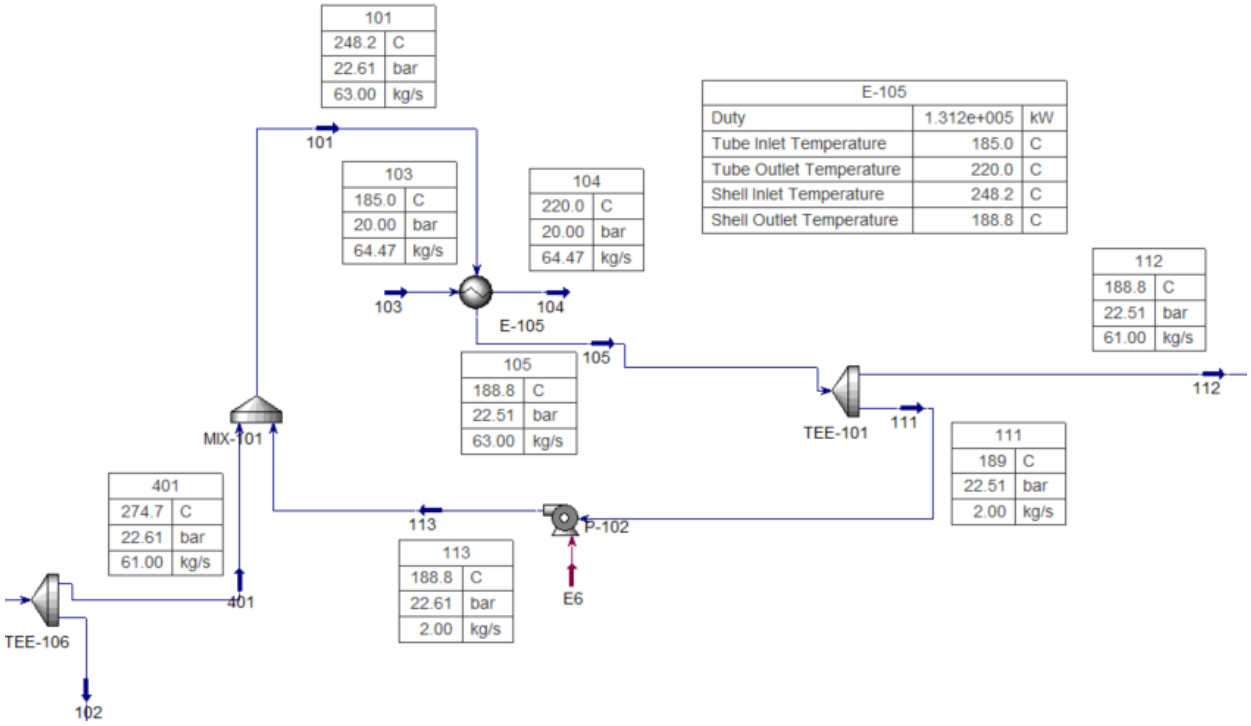

Figure 9. Heat exchanger integration for the HTGR on the NPP side supplying steam to be transported to the HTSE.

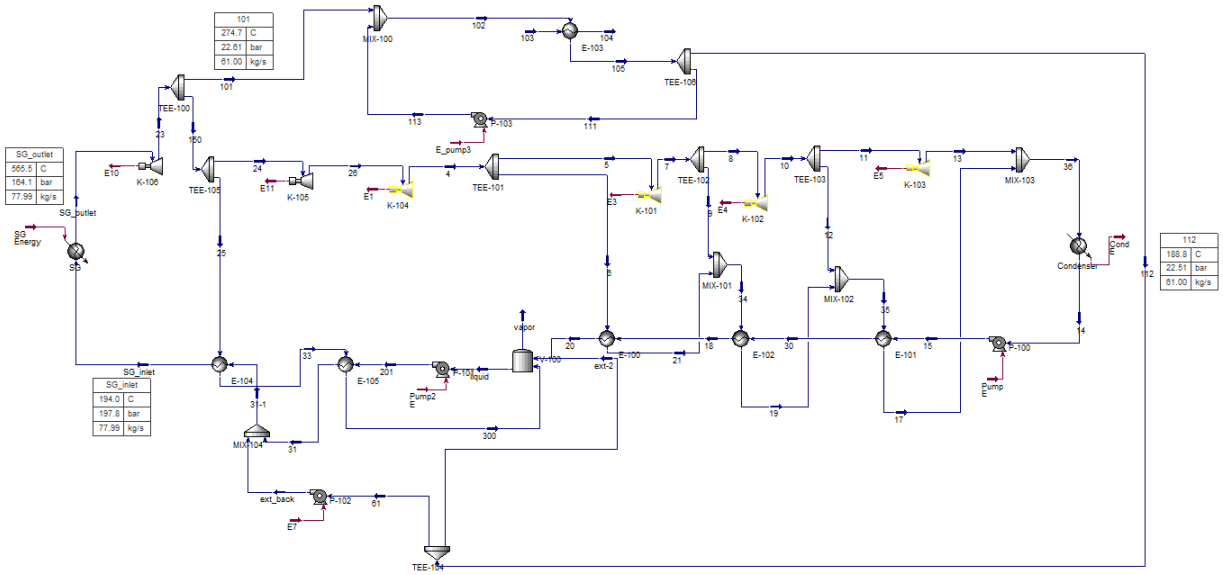

Figure 10. BOP for the HTGR integrated with HTSE.

In the CHP system, 131.2 MWth is consumed by process heat, leaving 68.8 MWth left for electricity production. Assuming a smaller turbogenerator system can still operate at an efficiency of 40%, the HTGR's initial efficiency (80/200), 27.65 MWe will be produced. In the HTGR case, the electricity produced from the CHP module is sufficient to reduce the overall number of HTGR modules by 1. The electricity demand for HTSE is 817.3 MWe and the electricity-only HTGRs and CHP module produce a surplus of 10.3 MWe as seen in Table 15.

4.3 Pathway-2: Elimination of Natural Gas Usage Using Reverse Water Gas Shift

4.3.1 Energy Requirement for High-Temperature Steam Electrolysis in Pathway-2

For Pathway-2, designed to produce 10,299 tpd of MeOH, a chemical facility would require thermal power inputs of 504.56 MWt (for HTSE) at 200°C and 142.66 MWt (for RWGS) at 600°C for a total of 3,595.47 MWe. The HTSE requirements are identical to the prior analysis because they can be linearly scaled for larger systems. The difference between the -Pathway-2 CHP configuration and the Pathway-1 CHP configuration lies in fully thermally integrated NPPs.

Based on the analysis in Section 4.2.2, the extraction flow to the HTSE heat exchanger creates an 87.6% thermodynamically efficient system, with the only loss due to the condensate return being too hot compared to the nominal feedwater conditions within the NPM. This value is safety-driven, and thus no changes are proposed that may impact it. Thus, a single NPM should be able to deliver 219 MWt of heat with effectively no system changes.

Regarding the HTGR configuration, based on the analysis in Section 4.2.3, the extraction flow to the HTSE heat exchanger is 100% efficient when downstream of the backpressure turbine since condensate returns entirely into the feedwater line. The backpressure turbine consumes 19.72% of the total energy, 39.44 MWe, with the system delivering the remaining energy to the HTSE heat exchanger (160.56 MWt). Thus, when more than 160.56 MWt of heat is required, multiple HTGRs would need to be included in the CHP configuration.

4.3.2 Reverse Water Gas Shift Reactor Heat

As stated in Table 9, the temperature that can be obtained from the NPP's steam header is lower than the temperature requirement at RWGS reactor of 600℃. Therefore, another method of applying heat (such as electric heating) or adding a heat augmentation unit is needed to directly supply heat from an NPP. An NPP CHP configuration that can deliver heat of 600℃ is a topic of future investigation. The HTGR can potentially have a more direct approach to delivering heat at 600℃ as outlet temperature of the core is 750℃. Without going to steam (which would likely require very high-temperature compressors), a high-temperature heat transfer fluid (HTF) could transport heat instead. This is also the target of future work as the RWGS can leverage a supplementary furnace.

Initially, it seems counterintuitive to use a furnace from a decarbonation point of view, but the system remains environmentally neutral from a CO_2 perspective. Based on current and novel methanol production processes, light gas containing byproduct CH_4 and unreacted H_2 will be separated during distillation. Currently, light gas is burned at the flare tower to reduce the GHG effect from methane or CH_4, which has 30 times higher GHG potentency than CO_2. Thus, light gas can be used as an alternative fuel for a supplementary furnace to heat the endothermic RWGS reactor. For Pathway--2, about 659 tpd light gas is expected to be produced, containing CH_4, H_2 and MeOH, at 127.49, 123.67, and 45.83 tpd, respectively. According to the Aspen Plus RGibbs reactor model, 187 MWth can be obtained by burning this light gas at 700℃, which is sufficient to meet the needs of the RWGS reactor (144.48 MWth).

5. PRELIMINARY THERMAL DELIVERY DESIGN

This section focuses on optimal designs of the piping and insulation systems. It is expected to achieve heat delivery from the boundary of advanced reactors to the boundary of methanol production sites within the context of the decarbonized pathways outlined in Sections 3 and 4. "Optimal design" refers to an insulated piping system that ensures meeting the desired heat-delivery objective at the lowest cost. In identifying the optimal designs for the heat-delivery scenarios discussed in Section 4, the following considerations were incorporated to suggest a practical, industry-standard-compliant solution suitable for commercial deployment:

1. Industry-standard pipe sizes and thicknesses or the nominal pipe sizes (NPS).
2. Design requirements as per ASME B31.1 (power piping), including maximum allowable stress and temperature of the selected pipe material, required thickness of pipes under pressure, and necessary pipe loops to accommodate thermal expansion.
3. Operational practices for high-temperature thermal systems and/or devices (e.g., heat exchanger), such as maximum or minimum velocity limits of the HTF.

It is important to note that the selection of HTF can significantly impact the insulated piping system design and its optimization. While the methodology and procedures proposed in this section can be extended to such an analysis, it is beyond the scope of direct interest covered in this report. Such analysis, including the impact of HTF selection on the heat-delivery design and associated cost, will be addressed in future work. The following subsections describe the methodology proposed to identify the optimal piping and insulation system designs for the thermal integration scenarios (NPP--HTSE) discussed in Section 4, and the preliminary optimization results.

5.1 Siting-based Constraints

The novel methanol pathways entail co-location of large-capacity HTSE, NPPs, and methanol reactors. Therefore, in support of the proposed decarbonized pathways, a dedicated hazard analysis is required across all possible pairs of three major technologies (i.e., between an NPP-HTSE, an NPP-methanol reactor, and an HTSE-methanol reactor).

Previous research at INL has reported a collection of hazard possibilities associated with placing a large-scale SOEC hydrogen production facility near an existing LWR [15]. For hazard analysis, HTSE capacity ratings of 100 MW, 500 MW, and 1,000 MW nominal (MW_e) energy ratings were considered. The colocation of these HTSE capacities with LWR NPPs was evaluated. The LWR was modeled as a 3,650 MW thermal (MW_t) plant rating that provides 1,200 MW electric power. For each HTSE capacity considered, seismic and wind events were assessed in this study to gauge if any impact on the HTSE will adversely affect the NPP. The previous study included 1,000 kg of hydrogen storage at the HTSE site. Last, the 1000 MW HTSE site was assumed to consist of two 500 MW sub-sites, feeding one transport pipeline.

Some of the core findings of the study are summarized below:

1. Limiting Factor: A pressure of 1,500 psi (103.4 bar) or higher within the hydrogen production header, which serves as a collector of hydrogen from multiple SOECs, was one of the major constraints for safe-distance siting. This pertains to a case wherein 1,000 MW high-temperature electrolysis facility draws 205 MWt steam from an LWR—200 MWt for thermal delivery and 5 MWt to account for potential delivery losses.
2. Risk-Informed Safe Siting Distance: For a 1,000 MW hydrogen production facility, a minimum safe distance of 681 meters was recommended. However, this distance has been approximated to 700 meters for the P&ID design proposed in this report.
3. Most Fragile Component at an NPP Site: The study scope used a detailed 1,000 MW HTSE model to assess potential hazards to the most fragile component of an NPP, which is the switchyard transmission tower. The switchyard is common across all NPPs, regardless of the reactor technology considered.

The investigation performed in Reference [15] is deterministic in nature and is expected to feed input parameters to a more detailed and sophisticated probabilistic risk assessment-based study for an HTSE-NPP hybrid. A similar research effort is underway to estimate a safe distance between the hydrogen production facility, and the site where the methanol reactor is to be placed.

5.2 Methodology

The piping system analysis, design, and optimization requires an integrated understanding of industry standards, ASME requirements, and operational practices for high-temperature systems. The objective is to find an optimal heat-delivery design that minimizes the capital and lifetime operating costs. The assessment is initiated by selecting the piping material, HTF, heat-delivery distance, and insulation material. Each selected component is chosen to efficiently function under operational conditions defined by the application case and must be well within component operational limitations. To scope the piping analysis, key assumptions are applied, which include: (1) uniform pipe diameter, (2) level piping (no change in elevation), (3) only frictional, form, and velocity change induced pressure losses (ΔP) are considered, (4) capital cost contributions from flanges, fittings, valves, and pumps, along with their varied ratings, are ignored in the piping stress and cost analysis, (5) piping system is above ground level avoiding shear stress from soil, and (6) pipe aging is ignored. For pressure loss, the velocity change can be induced by HTF density changes axially in the piping due to thermal energy loss.

For systems of low thermal energy transport, the density change is assumed negligible with installation of suitable insulation to prevent significant heat losses. However, for higher thermal energy transport systems, the allowable amount of heat loss can result in temperature changes of over 10°C and potentially increase density significantly depending on the HTF. To satisfy all applicable design standards, design requirements, and best practices, the logical flow and structure of the design optimization analysis is paramount. The first design standard or design requirement applied must be carefully selected because one design standard or design requirement could result in multiple constraints to the piping analysis. Figure 11 shows the logical flow and structure of the design optimization analysis proposed in this study, considering the flow of information and the objectives to design low-cost piping systems while meeting the design standards and requirements. The sections below expand on the logical structure described in Figure 11.

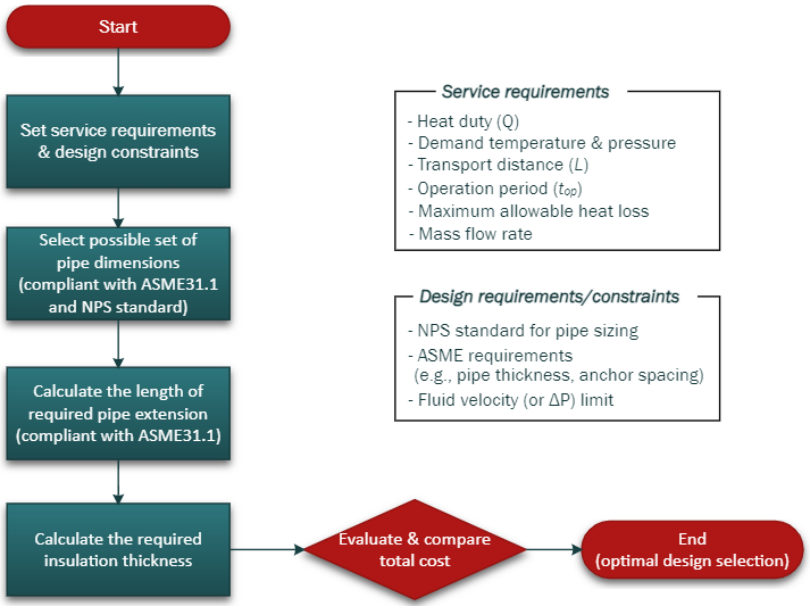

Figure 11. Logical structure of the heat delivery (piping) system analysis for optimization.

5.3 Requirements and Design Constraints

The first step is to determine the service requirements and design constraints. This includes the required heat-delivery duty (Q), source and sink demand temperature and pressure, transport distance (L), operation period, maximum allowable heat loss ($Q_{l,max}$), and mass flow rate ($\dot{m}$). These service requirements are also the minimal set of information to bound the heat-delivery design. Absence of this type of information will result in a design analysis of larger degrees of freedom and may yield non-optimized final designs. In the current approach, design optimization is constrained by standard industry pipe sizes, maximum and minimum velocity limits of the HTF, allowable operational temperature range, and heat-delivery system budget limitations. The combination of design standards and constraints will specify the range of applicable pipe outer-diameter sizes to investigate while applying ASME requirements to determine possible pipe dimensions suitable for commercial deployment. The service requirements and design constraints should be defined prior to initiating the thermal delivery design process.

5.4 Possible Set of Pipe Dimensions

The next step is to identify the possible set of NPS and their dimensions to meet the ASME requirement and design constraints for a given service requirement. For the selected pipe material, available NPS and schedules differ for the given operational requirements. ASME B31.1 has categorized and specified the allowable stresses in tables based on material and the operating temperature range. The two major stresses considered are sustained and displacement stresses. Sustained stress ranges are resulting forces from pressure, weight, or any other force applied along the defined piping system. Sustained pressure stresses are either internal or external influences that uniformly distribute along the piping. For internally and/or externally pressurized systems, ASME B31.3 provides the function to estimate the minimum pipe thickness (t_m) required and is shown in Equation (6).

$$t_m = \frac{PD_o}{2(SE \cdot W + Py)} + A \tag{6}$$

where

P = applied internal pressure (gauge pressure)

D_0 = outer pipe diameter

SE = maximum allowable stress at operational temperature

W = weld strength reduction factor

y = coefficient taking into account material properties and operational temperature

A = additional thickness to compensate for removed material such as installing mechanical joints and corrosion.

Sustained weight stress or other sustained loads are also called longitudinal stresses, and the sum shall not exceed the basic material allowable stress in hot conditions. The criterion for sustained loads (S_L) is shown in Equation (7).

$$S_L = \sqrt{\left[I_a\left|\frac{PD_O}{4t_n} + \frac{F_a}{A_p}\right| + \frac{\sqrt{(I_i M_{iA})^2 + (I_o M_{oA})^2}}{Z}\right]^2 + \left(\frac{I_t M_{tA}}{Z}\right)^2} \leq S_h \tag{7}$$

where

I_a = sustained longitudinal force index

t_n = pipe thickness

F_a = longitudinal force due to weight and other sustained loads

A_p = cross-sectional material area of the pipe

I_i = sustained in-plane moment index

M_{iA}= in-plane moment

I_o = sustained out-of-plane moment index

M_{oA} = out-of-plane moment

Z = nominal section modulus of pipe

I_t = sustained torsional moment index

M_{tA} = torsional moment

S_h = basic material allowable stress at the maximum temperature expected.

When of sufficient initial magnitude during system startup or extreme displacements, piping system stress ranges caused by thermal expansion and piping displacements, referred to as displacement stress, relax in the maximum stress condition as the result of local yielding or creep. For such non-sustained stresses, the stress is applied and relieved repeatedly creating cyclic stress. Depending on the number of cycles experienced during the lifetime of the piping system, the maximum allowable stress is reduced. This is known as the allowable displacement stress range (S_A). The criterion for displacement stress (S_E) is shown in Equation (8).

$$S_E = \sqrt{\left[\left|\frac{i_a F_C}{A_p}\right| + \frac{\sqrt{(i_i M_{iC})^2 + (i_o M_{oC})^2}}{Z}\right]^2 + \left(\frac{i_t M_{tC}}{Z}\right)^2} \leq S_A \quad (8)$$

where

i_a = axial force stress intensification factor

F_C = axial force range due to reference displacement load range

i_i = in-plane stress intensification factor

M_{iC} = displacement in-plane moment

i_o = out-of-plane stress intensification factor

M_{oC} = displacement out-of-plane moment

i_t = torsional stress intensification factor.

The allowable displacement stress range is calculated using the cyclic stress equation in Equation (9).

$$S_A = f(1.25S_c + 0.25S_h) \quad (9)$$

where

f = the cyclic stress range factor for the total number of equivalent reference displacement stress cycles

S_c = basic material allowable stress at the minimum temperature expected.

When the basic material allowable stress at the maximum temperature is greater than the determined sustained load stress, the difference between both parameters is added in Equation (10).

$$S_A = f(1.25S_c + 1.25S_h - S_L) \quad (10)$$

The cyclic stress range factor depends on the total number of equivalent reference displacement stress range cycles expected during the service life of the piping (N) and is limited to be equal or less than one as shown in Equation (11). The cause for such restraint leads to the concept of reduced allowable stress when the given piping system experiences multiple cycles of loading and unloading over the expected lifetime. Since a piping system cannot extend the allowable stress by having fewer cycles, the maximum allowable stress is when the system is cycle-load free, in other words, the cyclic stress range factor is equal to one.

$$f = \frac{6}{N^{0.2}} \leq 1.0 \quad (11)$$

A minimum value for the cyclic stress factor is 0.15, which results in an allowable displacement stress range for a total number of equivalent reference displacement stress range cycles greater than 10^8 cycles. When considering more than a single displacement stress range, whether from thermal expansion/contraction or other cyclic conditions, each significant stress range shall be computed. For the selected reference displacement stress range, the total number of equivalent reference displacement stress range cycles is in Equation (12).

$$N = N_E + \sum \left(q_i^5 N_i \right), q_i = \frac{S_i}{S_E} \text{ for } i = 1,2, \dots, n \tag{12}$$

where

N_E = number of cycles of the reference displacement stress range

N_i = number of cycles associated with displacement stress range

q_i = ratio of the displacement stress range

S_i = any computed stress range other than the reference displacement stress range.

For available NPS and associated schedules provided by vendors, pipe dimensions can also be determined by knowing the pipe material, pipe diameter, and pipe minimum thickness. It is recommended to cross check if the chosen pipe dimensions comply with the criteria in Equations (7) and (8). Given the operational temperature, pressure, and cyclic behavior, higher pipe schedules may be required.

5.5 Length of Required Pipe Extension

The range of pipe conditions that satisfy the ASME standards in B31.3 means the required extended pipe extension must be determined to accommodate displacement stress ranges for a given displacement length. Piping systems of uniform size have no more than two anchors and no intermediate restraints, and total number of cycles must be less than seven thousand. ASME B31.3 provides the approximate criterion to determine whether the selected pipe extension is within standards and is shown in Equation (13).

$$\begin{cases} (\text{U. S. Customary Units}) \dfrac{D_o Y}{(L-U)^2} \leq 30 \dfrac{S_A}{E_c} \\ (\text{SI Units}) \dfrac{D_o Y}{(L-U)^2} \leq 20800 \dfrac{S_A}{E_c} \end{cases} \tag{13}$$

where

E_c = modulus of elasticity at room temperature

L = developed length of pipe (total length of pipe taken along the pipe axial direction)

U = anchor distance (length of straight line between the anchors, not the axial distance along the pipe).

Using the stated criterion, the required extension length between two anchors can be calculated. As stated in ASME B31.3, all piping shall meet the following requirements with respect to flexibility:

- It shall be the designer's responsibility to perform an analysis unless the system meets one of the following criteria:
  - The piping system duplicates a successfully operating installation or replaces a system with a satisfactory service record.
  - The piping system can be adjudged adequate by comparison with previously analyzed systems.
  - Follows the criteria shown in Equations (7), (8), and (13).

- All systems not meeting the above criteria (or where reasonable doubt exists as to adequate flexibility between the anchor) shall be analyzed by simplified, approximate, or comprehensive methods of analysis that are appropriate for the specific case.
- Approximate or simplified methods may be applied only if they are used for the range of configurations for which their adequate accuracy has been demonstrated.
- Acceptable comprehensive methods of analysis include analytical methods, model tests, and chart methods that provide an evaluation of the forces, moments, and stresses caused by bending and torsion from the simultaneous consideration of terminal and intermediate restraints to thermal expansion of the entire piping system under consideration, and including all external movements transmitted to the piping by its terminal and intermediate attachments. Correction factors shall be applied for the stress intensification of curved pipe and branch connections, as provided by the details of these rules, and may be applied for the increased flexibility of such component parts.

Along with the assumptions previously stated and standards mentioned above, the required extension length starts with determining the allowable maximum anchor distance. As the distance between anchors is increased, the piping is subjected to higher weight loads and, depending on the pipe material, values can vary. Although there is suggested pipe-support spacing for stainless steel (SS) and carbon--based metals according to pipe outer diameter and thickness from ASME B31.3, the spacing is general and may not apply to all cases. The following approach that uses Equations (7), (8), and (13) as the thermal delivery piping system designs is a first-of-a-kind design, such that precedent cases of successfully operating systems under the proposed conditions do not exist. First, under the assumptions applied, Equation (7) is simplified due to no out-of-plane, torsional moments, or sustained external longitudinal forces.

$$S_L = I_a \left| \frac{PD_O}{4t_n} \right| + \frac{I_i M_{iA}}{Z} \leq S_h \tag{14}$$

The maximum in-plane moment at the center of the piping assumes a uniform weight load is derived:

$M_{iA} = \frac{wU^2}{8}$ where w is the uniform load in units of weight-force per distance [16]. Considering the weight contributions are from insulation, piping, and HTF, the maximum moment at the center is modified.

$$M_{iA} = \frac{U^2}{8}\left(w_{ins} + w_{pipe} + w_{HTF}\right) \tag{15}$$

where

w_{ins} = insulation weight load

w_{pipe} = pipe weight load

w_{HTF} = HTF weight load.

A visual representation of uniform load can be found in Figure 12. The maximum section modulus is derived to be $Z = \frac{I}{c}$ where I is the moment of inertia and c is the radial distance from the neutral axis (for this case, the center of the pipe). Added with the moment of inertia [16] and radial distance, the maximum section modulus is Equation (16).

$$Z = \frac{\pi}{32D_o}(D_o^2 - D_i^2) \tag{16}$$

where

D_i = pipe inner diameter.

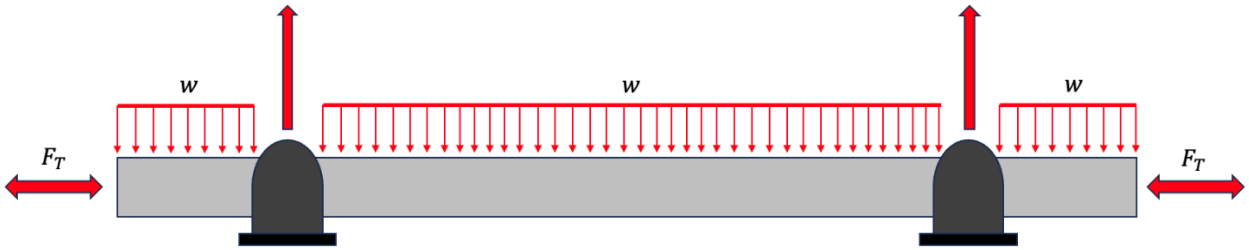

Figure 12. Leveled uniform-sized piping and the resulting uniform weight load.

Inserting Equations (15) and (16) into Equation (14) and reorganizing to be explicit about the anchor distance, the ranges of allowable anchor distances are derived.

$$U \leq \sqrt{\frac{\pi(D_o^4 - D_i^4)}{4D_0 I_i(w_{pipe} + w_{HTF} + w_{ins})}\left(S_h - \frac{I_a P D_O}{4t_n}\right)} \tag{17}$$

To abide to flexibility conditions defined in Equation (8), the allowable thermal stress must be ensured under the given operation conditions. The limiting factor that will dictate the maximum allowable displacement stress is the allowable displacement stress range. Acknowledging the only additional reference stress during operations is via thermal expansion and contraction, the displacement stress criterion is simplified.

$$S_E = \frac{i_a F_C}{A_p} = i_a \sigma_T \leq S_A \tag{18}$$

where σ_T is the thermal stress obtained when a known thermal strain (ε_T) and modulus of elasticity at operating temperature (E) is determined ($\sigma_T = E\varepsilon_T$).The thermal strain can be calculated by considering the linear thermal expansion coefficient (α_L) and temperature difference between operational temperature (T_{oper}) and piping installation temperature (T_{init}). Given the parameters provided and Equation (18), the final form of the allowable displacement stress is determined.

$$S_E = i_a E \varepsilon_T = i_a E \frac{U\alpha_L(T_{oper} - T_{init})}{U} = i_a E \alpha_L(T_{oper} - T_{init}) \leq S_A \tag{19}$$

The final form shown in Equation (19) provides insight on how the calculated displacement stress is independent of anchor distance. However, the allowable displacement stress range depends on anchor distance per Equation (10) if the criterion in Equation (7) is followed. Such an arrangement leads to complications. Depending on the modulus of elasticity at operational temperature and temperature difference, no matter how the anchor distance is shortened, criterion from Equation (19) may be impossible to satisfy. One important aspect to consider is the nature of displacement stress. As described in earlier sections, the displacement stress covers non-sustained applied stresses, such as cyclic stresses. During thermal delivery operations, there are anticipated HTF temperature fluctuations depending on dynamic operations and ambient condition changes. Thus, the temperature difference to use is not installation temperature but the minimum temperature ($T_{oper,min}$) anticipated during operations.

$$S_E = i_a E \alpha_L \left(T_{oper} - T_{oper,min}\right) \leq S_A \tag{20}$$

The extended length can now be determined by rearranging the criterion in Equation (13) to be explicit about the extension length.

$$\begin{cases} \text{(U. S. Customary Units)} L \geq \sqrt{\dfrac{D_o Y E_c}{30 S_A}} + U \\ \text{(SI Units)} L \geq \sqrt{\dfrac{D_o Y E_c}{20800 S_A}} + U \end{cases} \tag{21}$$

The developed length of pipe or total pipe length is adapted by using expansion loops, elbows, "Z" bends, or bellows joints, as required. For expansions loops, the extended amount of piping is offset by vertically or horizontally displacing a portion of the piping. Considering how the pipe is offset and returns to the original position as shown in Figure 13, the sum distance displaced is the extended pipe length. In this thermal delivery piping analysis, the expansion loop method was selected as it follows the assumption of no change in elevation. The best practice for expansion loops is to make the expansion loop height (H) half of the total pipe length, and the expansion loop width (W) half of the expansion loop height. The sum of the forward and return height, and width provides the total pipe length.

$$H = \frac{L}{2}, W = \frac{H}{2} \; where \; L = W + 2H \tag{22}$$

Since the analysis was restricted only between two anchors, the corrected HTF transport distance is the product of anchor numbers and extended lengths. To minimize the corrected HTF transport distance, greater anchor distances and reduced applied sustained stresses will be required.

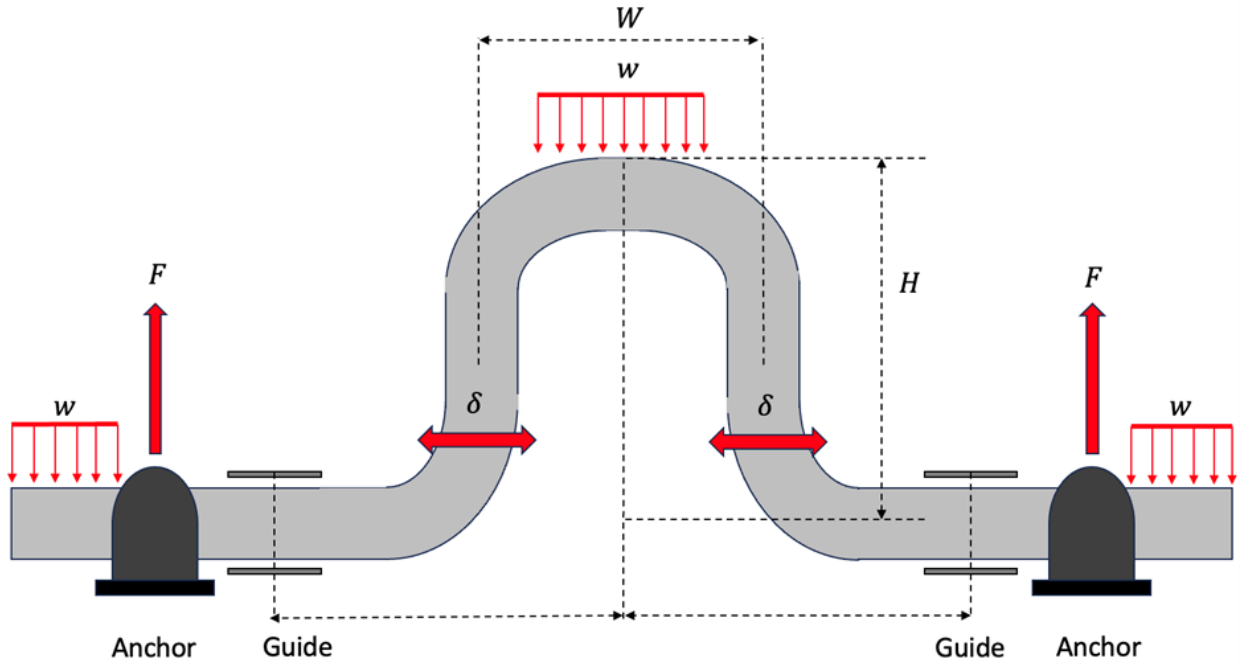

Figure 13. Visual representation of an expansion loop to deal with the extended length required based on ASME standards shown on Equation (21).

Another important feature of determining the treatment to extended pipe lengths is the analysis of pressure loss along the transport distance. Other than the friction pressure loss, the contribution from bends or so-called form loss is intensified when the number of expansion loops installed is increased. Later in Section 5.7, the effects of pressure loss to equivalent operational cost will be characterized.

5.6 Insulation Thickness Determination

After determining the possible set of NPS and their lengths as required by ASME B31.1, the next step is to determine the insulation thickness necessary to achieve the desired heat delivery. Once the insulation thickness is determined, the total heat loss over the heat-delivery distance (L), HTF temperature change, pipe-surface temperature, and other design values can be calculated. The insulation thickness can be determined based on one of two methods: (1) the first method involves pre-setting a target heat loss rate, while (2) the second method involves setting the maximum allowable heat loss based on the temperature difference between the heat source and the temperature demand. The first method is to preset the maximum allowable amount of heat loss compared to the amount of required heat duty (Q) and determine the thickness of the insulation material accordingly. The second method is to calculate the maximum allowable heat loss based on the heat-source temperature and the required temperature at delivery and determine the insulation thickness accordingly. Whichever method is used, the thermal resistance (R) should first be calculated based on the material properties of the components, (i.e., HTF, pipe, and insulation), as shown in Figure 14. The case study in this section used the second method to calculate the insulation thickness required to meet the desired heat-delivery purpose.

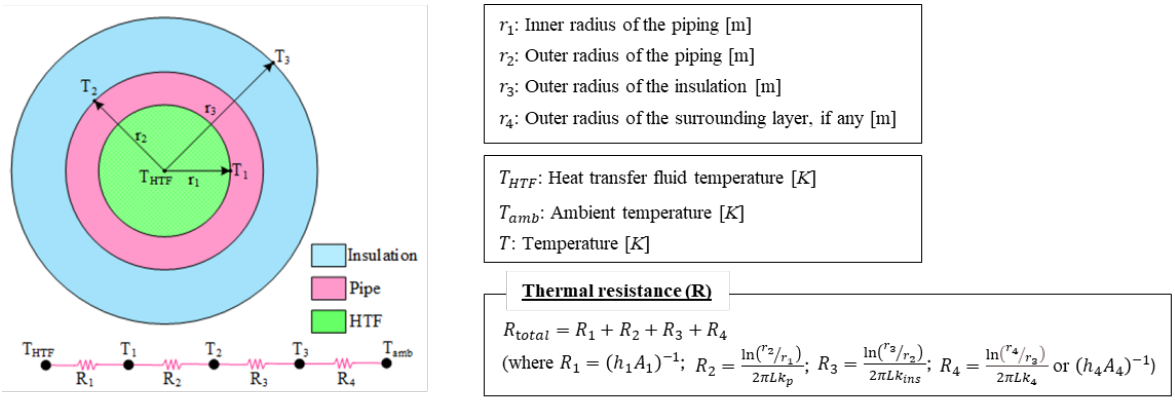

Figure 14. Cross-sectional view of insulated piping and thermal resistance (adapted from [17].

Figure 14 shows the cross-sectional view of the insulated piping structure along with the mathematical equation to calculate the thermal resistance. Given the total heat loss rate Q_{loss} [W], the total heat loss over an infinitesimal transport distance (dx) can be expressed as follows:

$$dQ_{loss}(x) = -\dot{m}C_{p,f}dT_x = \frac{\Delta T}{R_{total}} = \frac{T_f(x) - T_{amb}}{R_{total}} \tag{23}$$

where

$\dot{m}$ = mass flow rate of HTF [kg/s]

$C_{p,f}$ = specific heat of HTF [J/kg-K]

$T_f(x)$ = HTF temperature at the axial location x [K]

T_{amb} = ambient temperature [K]

R_{total} = total thermal resistance [K/W].

Each component of thermal resistance shown in Figure 14 (R_1, R_2, R_3, and R_4) can also be expressed over an infinitesimal transport distance (dx), leading to the following equation for the total thermal resistance over an infinitesimal transport distance (dx):

$$R_{\text{total}} = \frac{1}{h_1(2\pi r_1)dx} + \frac{\ln\left(\frac{r_2}{r_1}\right)}{(2\pi k_{pw})dx} + \frac{\ln\left(\frac{r_3}{r_2}\right)}{(2\pi k_{ins})dx} + \frac{1}{h_4(2\pi r_3)dx} \tag{24}$$

Combining Equations (23) and (24):

$$-\dot{m}C_p \frac{\mathrm{dT(x)}}{dx} = (T_f(\mathrm{x}) - T_{env})/(\frac{1}{h_1(2\pi r_1)} + \frac{\ln\left(\frac{r_2}{r_1}\right)}{(2\pi k_{pw})} + \frac{\ln\left(\frac{r_3}{r_2}\right)}{(2\pi k_{ins})} + \frac{1}{h_4(2\pi r_3)}) \tag{25}$$

Defining R_a=($\frac{1}{h_1(2\pi r_1)} + \frac{\ln\left(\frac{r_2}{r_1}\right)}{(2\pi k_{pw})} + \frac{\ln\left(\frac{r_3}{r_2}\right)}{(2\pi k_{ins})} + \frac{1}{h_4(2\pi r_3)}$), Equation (23) can be rewritten as:

$$-\dot{m}C_p R_a \frac{\mathrm{dT}_f(\mathrm{x})}{dx} = (T_f(\mathrm{x}) - T_{env}) \tag{26}$$

Equation (26) has the form of first-order differential equation and has the following analytic solution:

$$T_f(\mathrm{x}) = (T_{src} - T_{amb}) \exp\left(-\frac{x}{R_a \dot{m} C_p}\right) + T_{amb} \tag{27}$$

where

x = axial location along the pipe length

T_{src} = heat-source side temperature at $x = 0$. If the heat-source side temperature (T_{src}) and the temperature demand at $x = L$ (T_{demand}) are known, the maximum allowable heat loss over the distance L can be determined using the following equation:

$$Q_{loss,allowable} = -\int_{T_{src}}^{T_{demand}} \dot{m} C_{p,f} dT(x) \tag{28}$$

Assuming constant properties of HTF and constant mass flow rate, the above equation can be combined with Equation (23) to write:

$$Q_{loss,allowable} = -\dot{m}C_{p,f}\left[T_f(L) - T_{src}\right] = \frac{T_f(\mathrm{L}) - T_{env}}{\mathrm{R}_{total}} \tag{29}$$

where

$T_f(L)$ = HTF temperature at delivery (i.e., $x = L$).

Once a preset heat loss target is given as a percentage of the desired heat duty (first method) or the maximum allowable heat loss is calculated (second method), Equation (29) can be used to calculate the insulation thickness required.

5.7 Design Optimization

Upon identifying the feasible combinations of standard pipe sizes, required pipe-length extensions, and insulation thicknesses that meet design constraints, ASME requirements, and the given service requirements, the optimal piping design should now be selected from among the possible combinations. An optimal piping system, as previously defined, is one that achieves the desired heat-delivery purpose at the lowest possible cost. Thus, the objective function for optimization is set to minimize the total annual cost ($\underline{C_{total}}$) associated with constructing and operating the piping system. The annual total cost comprises the amortized capital costs of the pipe and insulation, along with the operating costs, which can be expressed as the following equation:

$$C_{total}(D_p, \theta) = C_p(D_p, \theta) + C_{ins}(D_p, \theta) + C_{\Delta P}(D_p, \theta) + C_{HL}(D_p, \theta) \tag{30}$$

where

C_{total} = annual total cost [$/yr]

C_p = amortized pipe cost [$/yr]

C_{ins} = amortized insulation cost [$/yr]

$C_{\Delta P}$ = operating cost due to pumping requirement [$/yr]

C_{HL} = operating cost due to heat loss [$/yr]

D_p = pipe diameter [m]

θ = pipe wall thickness [m].

5.7.1 Amortized Pipe Cost (Cp)

The capital cost of the pipe can be annualized by applying the amortization factor (*AF*), which accounts for the time value of money (i.e., interest). In principle, the *AF* is determined by the capital recovery factor (*CRF*), along with the costs associated with depreciation, property taxes, and income taxes, but the latter three factors are ignored in the current study [18,19]. With this simplification, the amortized pipe cost (C_p) can be calculated as:

$$C_p(D_p, \theta) = Z_p(D_p, \theta) \cdot AF(i, n) \tag{31}$$

where

Z_p = capital cost of the pipe [$]

AF = amortization factor

I = interest rate

n = economic operating period (or lifetime) of a piping system [*yr*].

The *AF* can be calculated using the following equation:

$$AF(i, n) = CRF(i, n) + \zeta \tag{32}$$

where *CRF* denotes the capital recovery factor $\left(= \frac{i(1+i)^n}{(1+i)^n - 1}\right)$ at interest rate *i* over the economic life *n* of a piping system, and ζ is a coefficient representing a portion of the fixed operation and maintenance cost [18].

5.7.2 Amortized Insulation Cost (Cins)

The amortized insulation cost can be calculated in the same way as for pipes:

$$C_{ins} = Z_{ins}(D_p, \theta) \cdot AF(i, n) \tag{33}$$

where

Z_{ins} = capital cost of the insulation [$].

5.7.3 Operating Cost Due to Pumping Requirement (C∆P) [$/yr]

Operating cost is determined by pumping cost to overcome the pressure loss during the flow of HTF as well as the electricity cost:

$$C_{\Delta P} = C_{el} \cdot \dot{W}_P \tag{34}$$

where

$\dot{W}_P$ = pumping power ($=\frac{\dot{m}\Delta P}{\rho \eta_p}$) [W]

η_p = pump efficiency, C_{el} is the specific cost for electricity [$/J].

The pressure loss, required in calculating pumping power and resultant operating cost, consists of two components: (i) frictional loss and (ii) minor (or form) loss. The total pressure loss over the heat-delivery distance L can be calculated using the following equation:

$$\Delta P = \frac{\rho_f \Delta v^2}{2} + \left(f \frac{L}{D_i} + K_{loss} \right) \frac{\rho_f u_f^2}{2} \tag{35}$$

where

Δv^2 = squared velocity difference induced by heat loss

F = friction factor

K_{loss} = minor loss coefficient (= 0.3 for 90-degree flanged elbow)

D_i = pipe inner diameter [m]

L = heat-delivery distance [m].

Once the required number of anchors (N_{anc}) are determined as described in Section 5.4, the number of expansion loops (N_{exp}) can be calculated as $N_{exp} = N_{anc} -$ two-dimensional expansion loop, as illustrated in Figure 13, each loop contains four 90-degree bends. As a result, the minor loss due to these bends over the heat-delivery distance L can be calculated as follows:

$$K_{loss} = 4 \cdot \sum_{i=1}^{N_{exp}} K_{loss,i} \tag{36}$$

where

$K_{loss,I}$ = minor loss coefficient at i_{th} expansion loop.

5.7.4 Operating Cost Due to Heat Loss (CHL) [$/yr]

$$C_{HL} = C_h \cdot \dot{Q}_{loss} \tag{37}$$

where C_h is the unit cost of available energy in the HTF [$/J]. The operating cost from heat loss (C_h [$/J]) can be considered as the cost required to offset the heat loss. For example, if heat loss occurs during heat delivery, it can be compensated for by increasing the pumping power (and thereby its cost) to achieve the desired heat-delivery purpose [18]. In this case, the additional pumping cost [$/J] required to offset the heat loss can be considered as operating cost due to heat loss. Considering the equations for pressure drop and mass flow rate, which are proportional to the square of the fluid velocity and fluid velocity, respectively, the pumping power ($\dot{W}_P$) is proportional to the third power of the fluid velocity. Consequently, if the mass flow rate ($\dot{m}$) is adjusted (i.e., increased) to offset the heat loss, it requires an approximately 3% increase in pumping power to compensate for a 1% heat loss. As a result, C_{HL} can be calculated as the following equation:

$$C_{HL} = C_h \cdot \dot{Q}_{loss} = C_{\Delta P} \cdot (3) \frac{\dot{Q}_{loss}}{Q} \tag{38}$$

6. RESULTS

The overall results show that using Pathway-1 and Pathway-2 for novel methanol synthesis configurations can significantly reduce the overall carbon dioxide emissions associated with methanol plants and subsequently in the downstream uses of methanol. The introduction of nuclear heat and electricity provides a 63% reduction in Scope-1 (on-site) emissions in Pathway-1. Based on the introduction of CO_2 as a feedstock in Pathway-2, CO_2 emissions are negative as the carbon is embedded in the methanol. Both Pathway-1 and Pathway-2 are tightly integrated into nuclear plants via the thermal sources required for HTSE. The P&IDs in Figure 15 and Figure 16 have been configured based on delivery of significant steam quantities relative to the size of the nuclear power plants. The specific results of the thermal transport calculations that provide the input for the thermodynamic calculations are presented in Section 6.2.

6.1 Piping and Instrumentation Diagrams

Figure 15 shows the P&ID diagram of the heat extraction system coupled with an HTGR for providing the methanol system HTSE with required steam. Note that it excludes auxiliary and emergency bypasses, drains, sludge, etc., which would be considered in more detailed engineering designs. The existing piping of the baseline steam cycle, which would only change by scaling down to a smaller system, is not pictured within the P&ID.

A junction that splits main steam between the HTSE feed and the nominal BOP system leads to a backpressure turbine. The outlet pressure of this turbine is reported in Section 4.2.3. There is still superheat in the system, and to reduce the total bypass steam flow, a steam attemperator is introduced to recycle some of the condensate return to create a nearly or fully saturated steam flow. This steam flow enters the HTSE-side's superheater before entering the vertically entered drum-type forced circulation boiler unit. This kind of unit should allow for a straightforward control of the HTSE steam generation rate via level control and provides a clear structure for steam generation in the system. The condensate then returns toward the HTGR BOP system where some is siphoned via pumping action back to act as an attemperator for the backpressure exhaust flow. A pump is installed to get the flow back to feedwater pressure and a small mixing tank combines the smaller electricity system with the return water.

The demineralized water in the HTSE plant is sourced and pumped through its heating system. A shell-and-tube condensing-type heat exchanger operating at low pressure will recover some heat in the methanol plant to provide some sensible heat into the demineralized water. The fluid will then enter the aforementioned drum-type boiler unit with steam being directed through the superheater unit prior to its transport to the HTSE system.

The proposed system has frequent sensor placements to monitor fluid temperatures and pressures, largely for control. Isolation valves are set in place to split the entire steam system into smaller operating sections, isolating the nominal electrical generation system and the thermal delivery system.

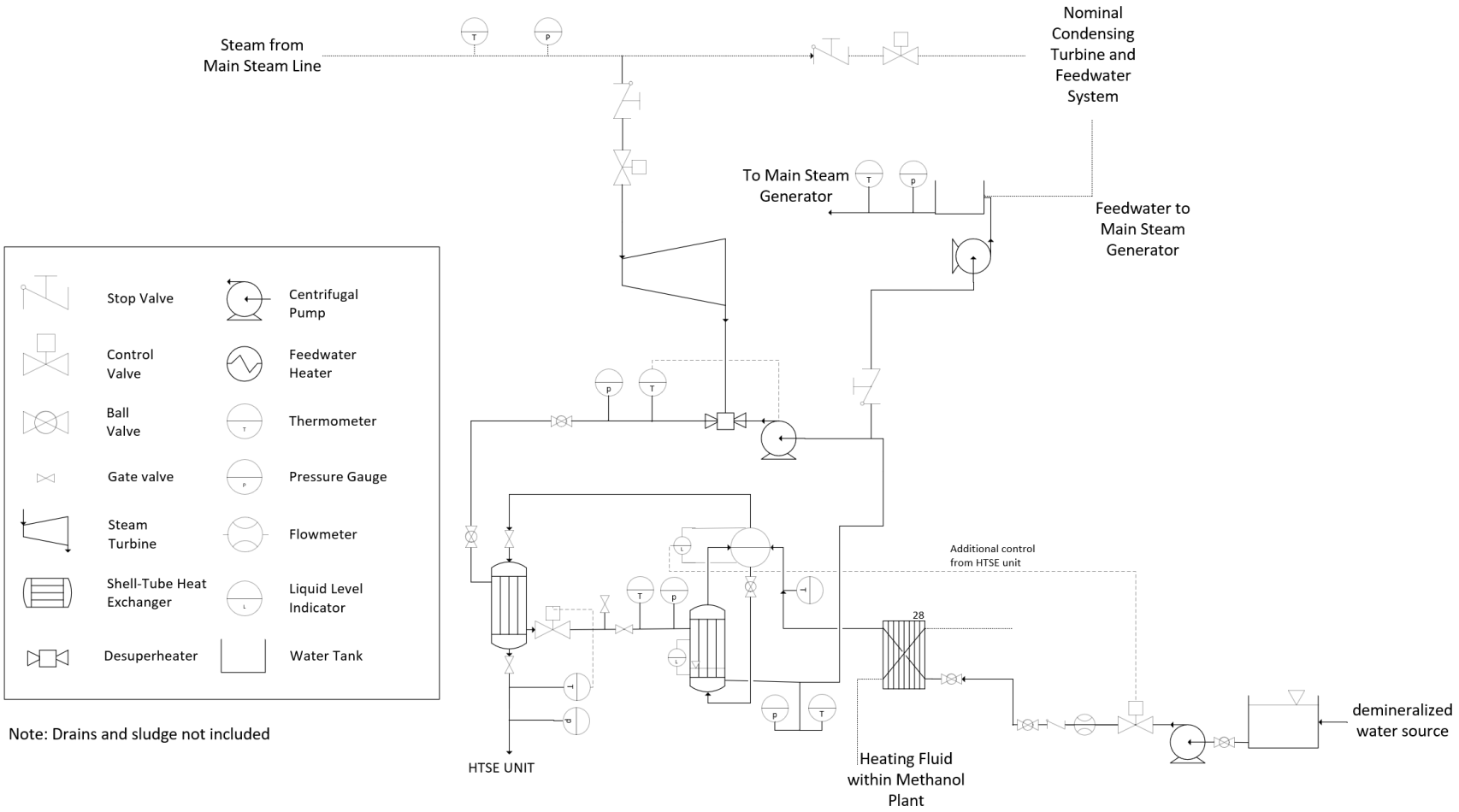

Figure 15. P&ID of the HTGR integration into the HTSE and methanol plant.

Figure 16 shows the P&ID diagram of a heat extraction system coupled with an LWR for providing the methanol system HTSE with required steam. Much of the system is similar to the HTGR configuration, and the same disclaimer applies—that the P&ID excludes auxiliary and emergency bypasses, drains, and sludge. The existing piping of the baseline steam cycle, which would only change by scaling down to a smaller system, is not pictured within the P&ID.

A junction that splits main steam between the HTSE feed and the nominal BOP system leads, unlike in the HTGR system, directly to the HTSE steam generation unit. This steam flow enters the HTSE-side's superheater before entering the vertically entered drum-type forced circulation boiler unit. This kind of unit should allow for straightforward control of the HTSE steam generation rate via level control and provides a clear structure for steam generation in the system. The condensate is then returned to the LWR nominal feedwater system just upstream of the steam generator after having been pumped to equilibrate pressure between the condensate and the nominal feedwater. A small plate-type heat exchanger is added to control temperature of the return water back into the feedwater system to ensure that it is in line with the nominal feedwater temperature.

The demineralized water in the HTSE plant is sourced and pumped through its heating system. A shell-and-tube condensing-type heat exchanger operating at low pressure will recover some heat in the methanol plant to provide some sensible heat to the demineralized water. The fluid then enters the drum-type boiler unit with steam being directed through the superheater unit prior to its transport to the HTSE system.

The proposed system has frequent sensor placements to monitor fluid temperatures and pressures, largely for control. Isolation valves are set in place to be able to split the entire steam system into smaller operating sections to isolate the electrical generation and the thermal power delivery systems.

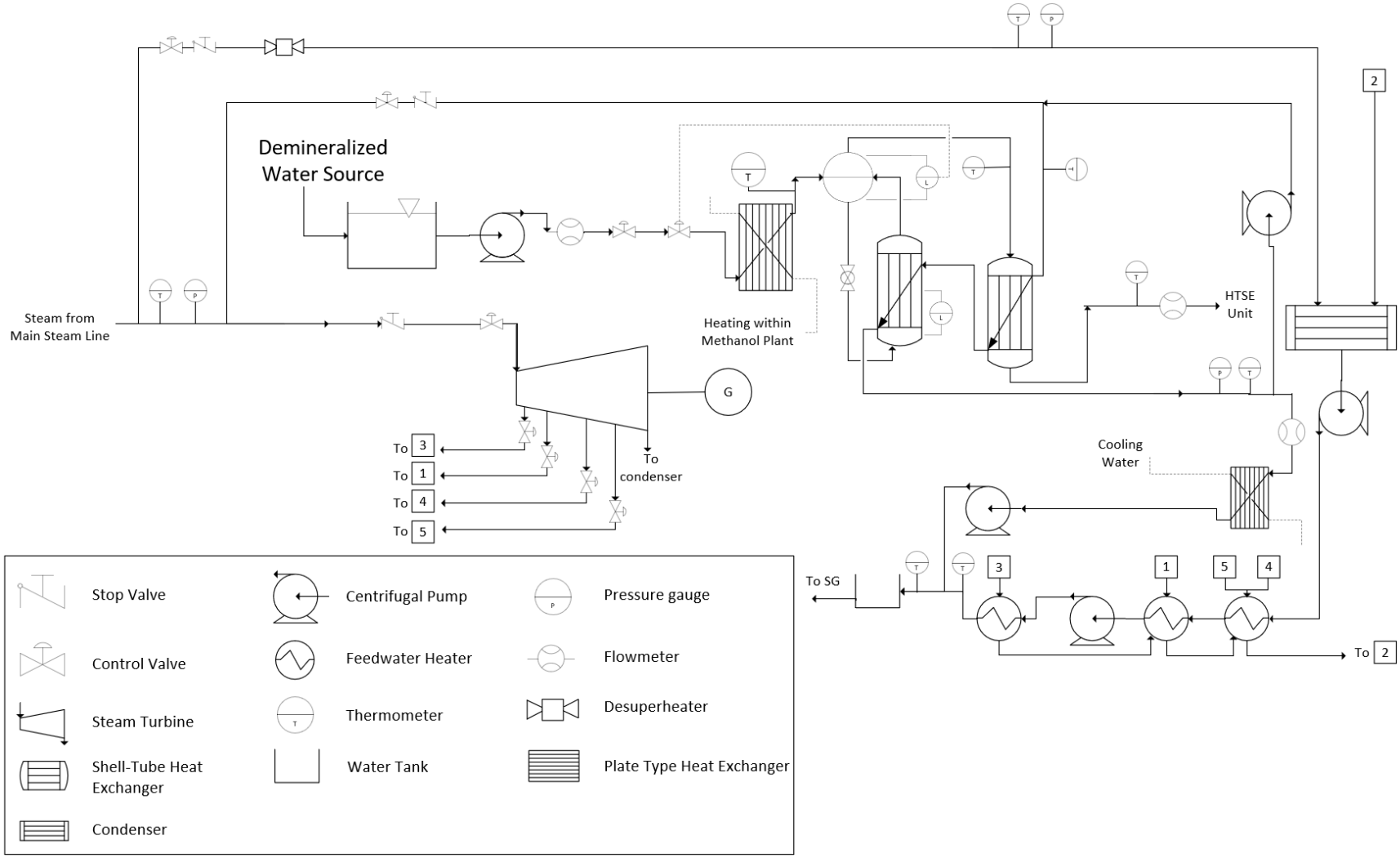

Figure 16. P&ID of the LWR integration into the HTSE and methanol plant.

6.2 Thermal Transport System

Sections 5.3 and 5.4 confirmed configurations of specific heat removal and supply from an NPP for methanol production processes. On both sides, heat removal (secondary steam line extraction) and supply (HTSE steam generation) are all from and to steam-centered systems. For this reason, the chosen HTF for heat delivery is steam. In the proposed thermal power delivery loop, the operating pressure is chosen to achieve efficient heat transfer through phase changes at heat removal and supply ends, delivering the desired heat duty at a specific mass flow rate with minimal pumping power. Choosing a suitable operating pressure will allow steam to be generated on the hot line and condensed liquid water in the cold line of the thermal power delivery loop. The operating pressure constraint is that the saturation temperature be within the heat exchanger's hot and cold temperature range. For saturation temperatures below the heat exchanger's cold operating temperatures, the HTF phase is constantly liquid. Alternatively, if saturation temperature rises above the heat exchanger hot operating temperatures, the HTF phase is constantly gas. In either case, the enthalpy difference is insufficient to supply enough heat for HTSE steam generation at the current mass flow rates of around 62 kg/s.

While working within the constraint for operational pressure, the constraint alone is insufficient for selecting a single-pressure value. There remains a variety of applicable pressure ranges that can accommodate the phase at the given heat exchanger operational temperatures. Considering the required heat duty and the threshold for heat loss in the thermal delivery loop, multiple scenarios at different operating pressures were tested to find cost-based optimal configurations. The determined optimized operational temperature and pressure conditions for the LWR and HTGR thermal delivery piping system are summarized in Table 10.

Table 10. Test matrix of thermal power delivery piping system analysis.

	Test No.	Reactor Type	Heat User	T_{src} [°C]	T_{demand} [°C]	P_{oper} [MPa]	Heat Duty [MW_{th}]	Mass Flow [kg/s]	HTF
Case 1	1, For.	LWR	HTSE	220	217.8	2.0	131.9	64.65	Steam
	1, Ret.	LWR	HTSE	186	185	2.0	131.2	64.65	Steam
Case 2	2, For.	HTGR	HTSE	220	217.8	2.0	131.9	64.65	Steam
	2, Ret.	HTGR	HTSE	186	185	2.0	131.2	64.65	Steam

The selection of insulation material is based on material density, operational temperature limits, thermal conductive properties, and cost per kilogram. Candidates for the insulation were mineral wool, aerogel, and polyimide rigid cellular materials. Properties of those materials are enlisted in Table 11. Mineral wool exhibited the best operating and cost performance for the designated allowable heat loss levels for each scenario in Table 10. Insulation imposes a cost on the entire system through two different mechanisms: the weight contribution to extending nominal pipe length and the required amount of insulation to prevent the heat loss threshold. The former non-linearly and the latter linearly affects the total cost, such that iteration is required in the optimization process. Aerogel performed slightly worse than mineral wool. For the given conditions, mineral wool was the optimal insulation material, but for different cases with higher temperatures and heat duty, the required insulation thickness of mineral wool may be larger than a meter. For these types of cases, aerogel may provide better insulation dimensions as the thermal conductivity at higher temperatures is significantly less than with mineral wool.

For piping material, SA213 stainless steel 316L was chosen. SS 316L is highly corrosion resistant and is used for high-temperature applications, such as high-pressure hydraulic servicing and heat exchangers. Although cast ductile iron and nickel alloy C-276 were candidates for the given operational conditions, further analysis of optimal piping is planned for future activities and will add to the dimensionality of the thermalpower delivery piping system design.

Table 11. Key insulation characteristics of selected candidates.[c]

	Mineral Wool [20-22]	Aerogel [22-24]	Polyimide Rigid Cellular [22, 24, 25]
Insulation Density (kg/m^3)	120–180	30–240	48–128
Insulation Operational Temperature Limits (°C)	<1200	<649	<315
Insulation Thermal Conductivity Coefficient (W/m·K)	0.023–0.1	0.023–0.048	0.023–0.048
Cost per kg ($/kg)	12.5*	266.7*	164.9*

Given the thermal power delivery requirements outlined in Table 10, the number of possible NPS pipe dimensions were determined to be 35 and 115 for the forward (from NPP to HTSE) and return (from HTSE to NPP) paths, respectively. These pipe dimensions are those that comply with the maximum velocity limit (currently set as 20 m/s) of the HTF (water/steam) and the ASME pipe thickness requirements at the operating pressure of the thermal delivery loop (20 bar). Different pipe diameters and thicknesses require different pipe length extensions as per ASME B31.1 (discussed in Section 5.5), affecting the total capital costs of the pipes. In addition, different pipe diameters will affect the pumping power required to achieve a specific mass flow rate of an HTF. Small-diameter pipes entail large pressure drops, requiring high pumping power and pumping costs. This is the opposite of the capital costs of the pipes. That is, as pipe size increases, pipe capital costs increase, whereas pumping costs decrease.

Figure 17 and Figure 18 show how the annualized total costs for forward and return path piping systems vary depending on the choice of pipe size and thickness, respectively. The numbers written next to the scatter plots for "Total Cost" in Figure 17 indicate the different schedules (thicknesses) for each nominal pipe size (omitted in Figure 18 to avoid cluttering the plots). Note that the capital costs for the pipe and insulation were annualized based on the AF assuming an interest rate of 5% and a piping system's operational life of 30 years (Section 5.7).

The calculated results of each cost component (i.e., capital, operating, and heat loss costs as described in Section 5.7) for each possible pipe dimension were combined to compare the annualized total cost, and the optimal case with the lowest total cost was selected among the possible pipe dimensions. The optimal NPS pipes selected on the forward and return paths are marked with red-dotted circles within the plots in Figure 17 and Figure 18, respectively. NPS 40 (standard schedule) was chosen for the forward path, and NPS 10 (schedule 5) was chosen for the return path. In the case of the return path, since the HTF was liquid water rather than steam, both the pipe size and the required pumping power were small, so the total cost was evaluated to be about one order lower than that for the forward path.

Table 12 summarizes the design characteristics, operating constraints, and cost details of the optimal piping system selected for a thermal delivery loop for the cases presented in Table 10. It includes key information such as pipe size and thickness, as well as the number of anchors to meet ASME loading requirements, total loop length required to meet ASME flexibility requirements, insulation thickness, and the estimated cost details. However, it is important to note that these are preliminary evaluation results assuming a very simplified thermal delivery loop design, as mentioned in Section 5.2.

[c] Superscripts of "*" represent values with unknown uncertainty due to different information provided by vendors. In this case, the values are placeholders until a specified vendor has been chosen [18].

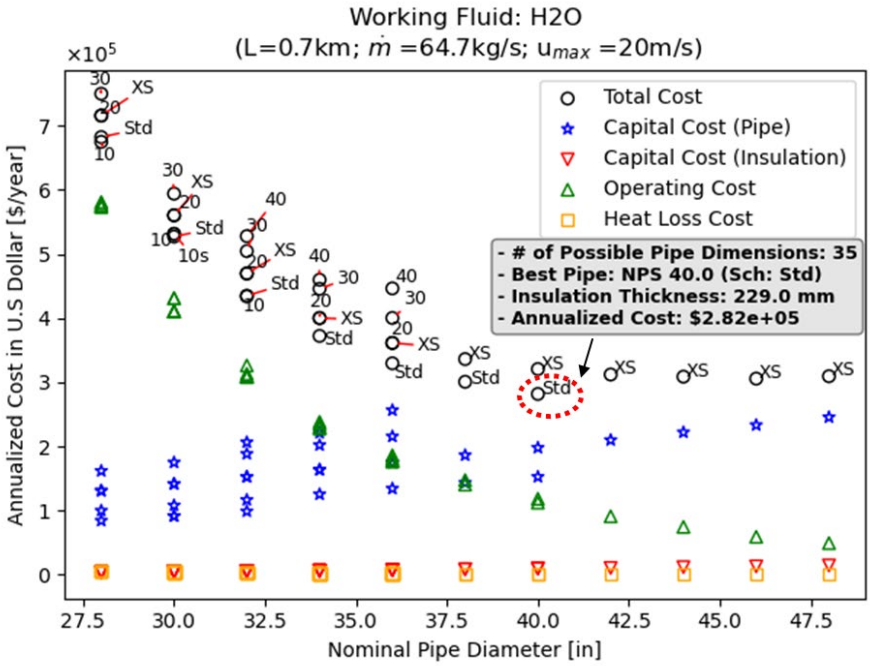

Figure 17. Cost variations of piping systems by nominal pipe diameter and schedule (forward path).

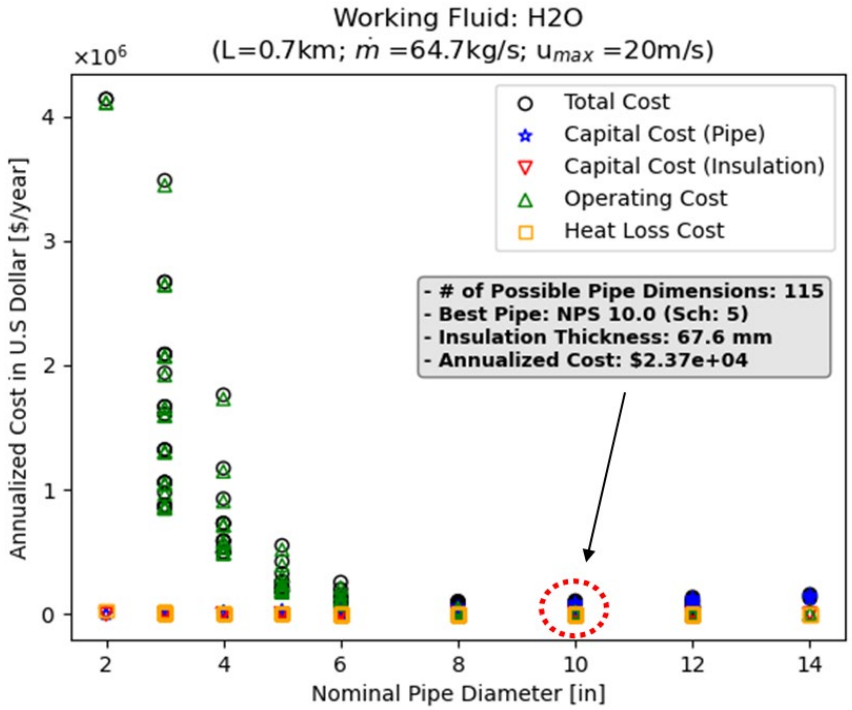

Figure 18. Cost variations of piping systems by nominal pipe diameter and schedule (return path).

Table 12. Preliminary optimization results for piping systems in Case 1 and Case 2.

Test Cases	Case 1 & Case 2	
	Forward	Return
Transport Distance (m)	700.0	700.0
Source Temperature (T_{src}, °C)	220	186.0
Demand Temperature (T_{demand}, °C)	217.8	185.0
Heat Delivery Pressure (bar)	20	20
Selected Pipe Dimension [Nominal Pipe Size (inch) / (Schedule)]	40 (Std)	10 (5)
Required Insulation Thickness (m)	0.331	0.109
Average Fluid Velocity (m/s)	8.43	1.32
Total Heat Loss (kW) / (%)	423.9 (0.3)	286.0 (0.2)
Lower Temperature Limit Constrained by Allowable Stress (°C)	167.7	133.3
Number of Expansion Loops Required	20	59
Anchor Spacing (m)	35	11.9
Corrected (or Extended) Pipe Length (m)	1211.4	1117.3
Required Pumping Power (kW)	74.9	6.29
Amortized Pipe Cost ($/year)	1.52×10^5	1.35×10^4
Amortized Insulation Cost ($/year)	9.75×10^4	7.43×10^2
Annual Operational Cost ($/year)	1.18×10^5	9.45×10^4
Annual Total Cost ($/year)	2.82×10^5	2.37×10^4

6.3 Summary of Methanol Integrated Plant Pathways

As detailed in Sections 2 and 3, the overall energy input to generate methanol increases with the introduction of nuclear energy by a small amount via Pathway-1 (4.07%) or Pathway-2 (3.6%). The primary change in the system is the change in the energy source from feedstock NG to heat and electricity.

The nominally analyzed system in this report generates 10,927 tpd of MeOH. Table 13 shows the overall energy requirements, inputs and outputs, and CO_2 emissions each for the nominal reference methanol model, Pathway-1, and Pathway-2. The CO_2 emissions are evaluated to be negative in Pathway-2 for the scope-1 emissions via the CO_2 being embedded within the methanol. Even any local emissions at that plant would necessarily be sourced from the external CO_2 source, and so from a scope-1 standpoint, emissions would be negative. When including an assumed methanol usage factor of 44/32 kg-CO_2/kg MeOH, Pathway-2 becomes a circular net-zero pathway while the carbon intensity of the nominal system and Pathway-1 increase. Further studies will likely be conducted to estimate lifecycle emissions of each pathway. It is possible to get preliminary estimates, but due to the robust nature of the values presented in Table 13, it would be imprecise to include approximations for scope-2 and scope--3 emissions associated with the full methanol synthesis lifecycle of Pathway-1 and Pathway-2.

Table 13. Summary of overall methanol Pathway-1 and Pathway-2 energy and emission outputs.

	Reference Methanol Model Burning NG as Fuel	Burning H_2 as Fuel from HTSE (Pathway-1)	RWGS + Selexol (Pathway-2)
Energy Requirement			
Feedstock	28.24 GJ/tonne MeOH	28.24 GJ/tonne MeOH	—
Fuel	5.91 GJ/tonne MeOH	—	—
Heat requirement	—	6.46 GJ/tonne MeOH	5.51 GJ/tonne MeOH
Electricity requirement	—	1.04 GJ/tonne MeOH	29.87 GJ/tonne MeOH
Total Energy requirement	34.15 GJ/tonne MeOH	35.54 GJ/tonne MeOH	35.38 GJ/tonne MeOH
Reference Methanol Model: Input and Output			
MeOH production	10,927 tpd	10,927 tpd	10,299 tpd
Feedstock	6,209 tpd of NG 7,200 tpd of treated H_2O 3,600 tpd of O_2	6,209 tpd of NG 7,200 tpd of treated H_2O 3,600 tpd of O_2	15,000 tpd of CO_2 19,170 tpd of treated H_2O 23,234 tpd of Air
Raw material for heating at furnace	1,300 tpd of NG	4,800 tpd of H_2O ($\rightarrow$539 tpd of H_2)	N/A
CO_2 emission			
Scope-1 plus CO_2 utilization	0.524 kg CO_2 / kg MeOH*	0.195 CO_2 / kg MeOH*	-1.375 kg CO_2 / kg MeOH*
Scope-1 plus CO_2 utilization and methanol use	1.899 kg CO_2 / kg MeOH*	1.570 CO_2 / kg MeOH*	0.00 kg CO_2 / kg MeOH*

* Assumed that all material containing carbon atom at the gaseous outlet are completely combusted and turned into CO_2 including methanol.

6.4 Nuclear Capacities

This section leverages the values and analysis in Sections 4.2 and 4.3 to show the quantity and configurations of NPPs required for the systems.

6.4.1 Pathway-1 HTGR and LWR Capacities

To fully power Pathway-1, there will need to be one CHP VOYGR module (with a heat-only configuration—120MWth would need to be reduced in power, wasted, or another application found for it) and 11 electricity-only modules to meet the required electricity demand of 817.3 MWe as seen in Table 14. In the CHP, 131.2 MWth is consumed by process heat, leaving 118.8 MWth left for electricity production. Assuming a smaller turbine island could still operate at an efficiency of 30.8%, the VOYGR nominal efficiency (77/250), 36.6 MWe will be produced, and the CHP module will operate with an overall efficiency of 67%. The CHP NPM does not produce enough electricity in addition to 10 NPM modules to fully produce the electricity needed for HTSE. Thus, 11 electricity-only NPMs are required in conjunction with the one CHP module for Pathway-1. Overall, this system produces 66.3 MWe surplus.

Table 14. Integration needs for HTSE using LWR. The total electricity demand is 817.3 MWe.

Type of Reactor	Thermal Heat Output (MWth)	Electricity Output (MWe)	Number of NPMs Needed	Electricity Total from Reactor Type (MWe)
CHP	131.2	36.6	1	36.6
Electricity Only	0	77	11	847
Totals	131.2	—	—	883.6

In the HTGR case, the electricity produced from the CHP NPM is sufficient to reduce the overall number of HTGR modules by 1. One CHP module can generate the needed heat requirements. The total electricity demand for HTSE is 817.3 MWe and the ten electricity-only HTGRs and CHP module produce a surplus of 10.3 MWe as seen in Table 15.

Table 15. Integration needs for HTSE using HTGR. The total electricity demand is 817.3 MWe.

Type of Reactor	Thermal Heat Output (MWth)	Electricity Output (MWe)	Number of NPMs Needed	Electricity Total from Reactor Type (MWe)
CHP	131.2	27.6	1	27.6
Electricity Only	0	80	10	800
Totals	131.2	—	—	827.6

6.4.2 Pathway-2 HTGR and LWR Capacities

Table 16 details the number of NPMs or Xe-100 modules needed to entirely deliver the 504.56 MWt and 3595.47 MWe HTSE demands for Pathway-2.

Leveraging the heat-delivery efficiencies (calculated in Section 4.2.2) of 87.6%, 575.7 MWt of rated NPM must be leveraged to transport the 504.56 MWt needed for HTSE. At 250 MWt per module, three modules would need to be used in heat-only or CHP configuration to supply the necessary heat. With the excess 174.3 MWt, these combined modules would also produce 53.68 MWe at nominal efficiency. To cover the remaining HTSE demand, another 46 NPMs would be required for electricity generation, bringing the system to 49 total NPMs.

Four HTGRs in entirely back pressure configurations or in CHP (split between back pressure turbine and condensing turbine) configurations would be needed to generate the HTSE steam as a fully back pressure turbine system generates 39.44 MWe and 160.56 MWt. An additional 43 Xe-100 modules would be needed to generate the remaining electricity, bringing the total of Xe-100 modules also to 47. The values for HTGR and LWR are summarized in Table 16, with CHP and heat-only reactors averaged together for the NPM or Xe-100.

Table 16. NPM and Xe-100 energy distribution totals for Pathway-2.

Type of Reactor	Thermal Heat Output (MWt)	Electricity Output (MWe)	Number of NPMs Needed	Electricity Total from Reactor Type (MWe)
NPM: CHP & Heat	168.2	17.9	3	53.68
NPM: Electricity Only	0	77	46	3542
NPM: Totals	504.56		49	3595.68
Xe-100: CHP & Heat	126.14	48.14	4	192.56
Xe-100: Electricity only	0	80	43	3440
Xe-100: Totals	504.56		47	3632.56

The overall methanol system is very large, so the total amount of nuclear small modular reactors required to provide the overall heat and electricity should not be surprising. At these quantities, it may be prudent to investigate mixes of small modular reactors and traditional large reactors in future analyses depending on reliability assumptions.

7. CONCLUSIONS AND AVENUES FOR FUTURE WORK

Introduction of nuclear energy into methanol plants will require some reconfiguration of the existing systems. The most straightforward change proposed in this work will be to replace NG in the steam-methane reforming system, getting heat from nuclear reactors via hydrogen burning. The entire replacement of NG will require a greenfield installation of the RWGS + Selexol systems to prepare syngas for the installation. There are compelling emissions benefits to motivate this investment though, as the methanol plant emissions become negative due to CO_2 consumption.

It is clear from this work that replacing large quantities of energy requires larger quantities of energy as efficiencies decline and more losses are introduced into the system. Nuclear power can generate the necessary energy required and replace significant quantities of NG energy at the energetic cost of leveraging electricity instead of the chemical energy held within NG. Future work should build upon the engineering analysis described in this work to extend the preliminary scope-1 emissions testing into a full lifecycle analysis of total emissions, including methanol consumption (which is not always combusted and thus may actually capture some carbon). Additionally, there is an opportunity for high-temperature heat delivery within Pathway-2 that is not yet detailed. It should be possible to provide the energy needed at 600°C in the RWGS system from a nuclear plant, especially an HTGR or via nuclear-generated electricity. Uses for the chemical energy leveraged to maintain RWGS temperature will need to be identified, as well as the impacts on the nuclear supply system that will provide such relatively high-temperature heat.

The methods and models for calculating the thermodynamic and economic costs of thermal delivery over distance should be leveraged to generate not only specific heat integration costs, but also generalized rules for HTF selection in different conditions. The capability of the models should be leveraged to calculate across different HTFs, conditions, and distances.

The overall results of this work will be used in technoeconomic analysis calculations to determine key figures of merit regarding the adoption of nuclear energy into the methanol industry. These analyses can also inform decarbonization priorities by identifying the avoided cost of carbon compared to other industries to identify economic priorities.

8. FUNDING ACKNOWLEDGMENTS

This work was supported by the IES program at Idaho National Laboratory under the Department of Energy Operations contract no. DEAC0705ID14517.

9. REFERENCES

1. Idaho National Laboratory. 2012. "Nuclear-Integrated Methanol-to-Olefins Production Analysis." Idaho Falls, ID.
2. Idaho National Laboratory. 2014. "Biomass/Coal to Methanol and Methanol to Gasoline Process Model." Idaho Falls, ID.
3. Energy Information Administration. 2012. "U.S. dry natural gas production growth levels off following decline in natural gas prices." https://www.eia.gov/todayinenergy/detail.php?id=6630.
4. American Chemistry Council. 2020. "Methanol production in the United States from 1990 to 2019 (in 1,000 metric tons)." Statista, Graph. Accessed May 2024.
5. Methanol Institute. 2022. "Carbon Footprint of Methanol.". https://www.methanol.org/wp-content/uploads/2022/01/carbon-footprint-of-methanol-paper_1-31-22.pdf.
6. Jin, C., C. Yang, and F. Chen. 2011. "Characteristics of the Hydrogen Electrode in High Temperature Steam Electrolysis Process." *Journal of The Electrochemical Society* 158(10): B1217. https://iopscience.iop.org/article/10.1149/1.3615992.
7. Wendt, D. S., L. T. Knighton, and R. D. Boardman. 2022. "High Temperature Steam Electrolysis Process Performance and Cost Estimates." INL/RPT-22-66117, Idaho National Laboratory, Idaho Falls, ID. https://doi.org/10.2172/1867883.
8. Joseck, F. et al. n.d. "Thermal Integration of Advanced Nuclear Reactors with a Reference Refinery, Methanol Synthesis, and Wood Pulp Plant." Idaho National Laboratory, Idaho Falls, ID.
9. Greenhouse Gas Protocol. n.d. "FAQ." World Resources Institute and wbcsd, Eds., ed. https://ghgprotocol.org/sites/default/files/standards_supporting/FAQ.pdf
10. González-Castaño, M., B. Dorneanu, and H. Arellano-García. 2021. "The reverse water gas shift reaction: a process systems engineering perspective." *Reaction Chemistry & Engineering* 6(6): 954–976. https://doi.org/10.1039/D0RE00478B.
11. Zhang, R. et al. 2021. "Tuning reverse water gas shift and methanation reactions during CO_2 reduction on Ni catalysts via surface modification by MoO_x." *Journal of CO2 Utilization* 52: 101678. https://doi.org/10.1016/j.jcou.2021.101678.
12. Kim, D. H., J. L. Park, E. J. Park, Y. D. Kim, and S. Uhm. 2014. "Dopant Effect of Barium Zirconate-Based Perovskite-Type Catalysts for the Intermediate-Temperature Reverse Water Gas Shift Reaction." *ACS Catalysis* 4(9): 3117–3122. https://doi.org/10.1021/cs500476e.
13. Vanden Bussche, K. M., and G. F. Froment. 1996. "A Steady-State Kinetic Model for Methanol Synthesis and the Water Gas Shift Reaction on a Commercial $Cu/ZnO/Al_2O_3$Catalyst." *Journal of Catalysis* 161(1): 1–10. https://doi.org/10.1006/jcat.1996.0156.

14. Doctor, R. D., J. C. Molburg, P. Thimmapuram, G. F. Berry, C. D. Livengood, and R. A. Johnson. 1993. “Gasification combined cycle: Carbon dioxide recovery, transport, and disposal.” *Energy Conversion and Management* 34(9): 1113–1120. https://doi.org/10.1016/0196-8904(93)90060-N.
15. Vedros, K. G., R. Christian, and C. M. Yang Hui Otani. “Expansion of Hazards and Probabilistic Risk Assessments of a Light-Water Reactor Coupled with Electrolysis Hydrogen Production Plants.” NL/RPT-23-74319, Idaho National Laboratory, Idaho Falls, ID. https://doi.org/10.2172/1998560.
16. Budynas, R. G. and A. M. Sadegh. 2020. *Roark's Formulas for Stress and Strain*, McGraw-Hill Education, New York, NY 9th Edition.
17. Balderrama Prieto, S. A., E. K. Worsham, and J. S. Yoo. 2023. “Identification and Evaluation of Thermal Transport Components for Integrated Energy Systems.” INL/RPT-23-75722, Idaho National Laboratory, Idaho Falls, ID. https://doi.org/10.2172/2242411.
18. Öztürk, İ. T., H. Karabay, and E. Bilgen. 2006. “Thermo-economic optimization of hot water piping systems: A comparison study.” *Energy* 31(12): 2094–2107. https://doi.org/10.1016/j.energy.2005.10.008.
19. Wepfer, W. J., R. A. Gaggioli, and E. F. Obert. 1979. “Economic Sizing of Steam Piping and Insulation,” *Journal of Engineering for Industry* 101(4): 427–433. https://doi.org/10.1115/1.3439532.
20. ASTM C726-17. 2017. “Specification for Mineral Wool Roof Insulation Board.” ed: ASTM International, 2017.
21. ASTM C1728-23. 2021. “Test Method for Steady-State Thermal Transmission Properties by Means of the Heat Flow Meter Apparatus,” ed: ASTM International, 2021.
22. ASTM C335M-23. 2023. “Test Method for Steady-State Heat Transfer Properties of Pipe Insulation,” ed: ASTM International, 2023.
23. ASTM C1728-23. 2023. “Specification for Flexible Aerogel Insulation,” ed: ASTM International, 2023.
24. ASTM C518-21. 2021. “Test Method for Steady-State Thermal Transmission Properties by Means of the Heat Flow Meter Apparatus,” ed: ASTM International, 2021.
25. ASTM C1594-23. 2023. “Specification for polyimide Rigid Cellular Thermal Insulation,” ed: ASTM International, 2023.